GEOLOGICA CARPATHICA, JUNE 2014, 65, 3, 207–225 doi: 10.2478/geoca-2014-0015

Genetic relationships between skarn ore deposits and magmatic activity in the Ahar region, Western Alborz, NW Iran

HABIB MOLLAI[1]✉, GEORGIA PE-PIPER[2] and RAHIM DABIRI[1]

[1]Department of Geology, Mashhad Branch, Islamic Azad University, Mashhad, Iran;
✉mollai@mshdiau.ac.ir
[2]Department of Geology, Saint Mary's University, Halifax, Nova Scotia, Canada B3H 3C3

(Manuscript received January 27, 2013; accepted in revised form March 11, 2014)

Abstract: Paleocene to Oligocene tectonic processes in northwest Iran resulted in extensive I-type calc-alkaline and alkaline magmatic activity in the Ahar region. Numerous skarn deposits formed in the contact between Upper Cretaceous impure carbonate rocks and Oligocene–Miocene plutonic rocks. This study presents new field observations of skarns in the western Alborz range and is based on geochemistry of igneous rocks, mineralogy of the important skarn deposits, and electron microprobe analyses of skarn minerals. These data are used to interpret the metasomatism during sequential skarn formation and the geotectonic setting of the skarn ore deposit related igneous rocks. The skarns were classified into exoskarn, endoskarn and ore skarn. Andraditic garnet is the main skarn mineral; the pyroxene belongs to the diopside-hedenbergite series. The skarnification started with pluton emplacement and metamorphism of carbonate rocks followed by prograde metasomatism and the formation of anhydrous minerals like garnet and pyroxene. The next stage resulted in retro gradation of anhydrous minerals along with the formation of oxide minerals (magnetite and hematite) followed by the formation of hydrosilicate minerals like epidote, actinolite, chlorite, quartz, sericite and sulfide mineralization. In addition to Fe, Si and Mg, substantial amounts of Cu, along with volatile components such as H_2S and CO_2 were added to the skarn system. Skarn mineralogy and geochemistry of the igneous rocks indicate an island arc or subduction-related origin of the Fe-Cu skarn deposit.

Key words: Late Cenozoic, granodiorite, magmatic, skarn, garnet, epidote, sulfide, Iran.

Introduction

Magmatic activities and the Alborz-Azerbaijan mountain range in the northern to northwestern parts of Iran are the results of the collision of segments of Gondwanaland and the Arabian plate with the Eurasian plate. Volcanic rocks occurred mainly as a result of extension or tension related to the continental rifting, or subduction of the developed oceanic lithosphere under the continental lithosphere (Dilek et al. 2010; Tarkhani et al. 2010). Most of the important Cu, Cu-Fe and Fe skarn in the world are related to subduction and collision producing I-type magmatic activities (Atkinson & Einaudi 1978; Einaudi et al. 1981; Einaudi & Burt 1982; Meinert 1992; Groves et al. 1998; Boztuğ et al. 2003; Chen et al. 2007). Skarn deposits in the Gharah Dagh Formation (part of Western Alborz), northwestern Iran, are the result of extensive I-type calc-alkaline and alkaline magmatic activity of Late Eocene–Oligocene and Oligo–Miocene age in the Ahar region. This magmatic activity was responsible for the contact metasomatic mineralization as well as the porphyry-type copper occurrences in NW Iran. As Figure 1 shows, the Gharah Dagh Formation is one of the important metallogenic provinces of the East Mediterranean Copper-Molybdenum belt (Bazin & Hübner 1969; Superceanu 1971; Rolland et al. 2009; Jamali et al. 2010). The associated intrusive bodies occur as batholiths as well as stocks, ranging in composition from quartz monzodiorite to granite, and the Ahar Batholith is the largest early Oligocene intrusion in the Gharah Dagh–Tarom plutonic belt (Lescuyer 1976). The important skarn deposits in these areas are Mazraeh skarn, Sungun skarn porphyry and Anjered skarn deposits. The Sungun copper skarn porphyry deposit located 85 kilometers west of Ahar town is associated with a smaller diorite of Oligocene age (Fig. 2), whereas in the Mazraeh and Anjered area several smaller skarn deposits, are found at the margin of the Ahar Batholith.

The aim of this paper is to present new field observations of skarns in the western Alborz of northwestern Iran; to describe the petrography, mineralogy, mineral chemistry and geochemistry of the important related rocks; and to use these data to interpret the sequence and the geotectonic setting of skarn formation. In addition this paper documents correlations between intrusion composition and the metal contents of associated skarns.

Methods

Field work included geological mapping, delineating the igneous bodies, the skarn and marble contact. Sampling traverses were done across the skarn and host rocks. More

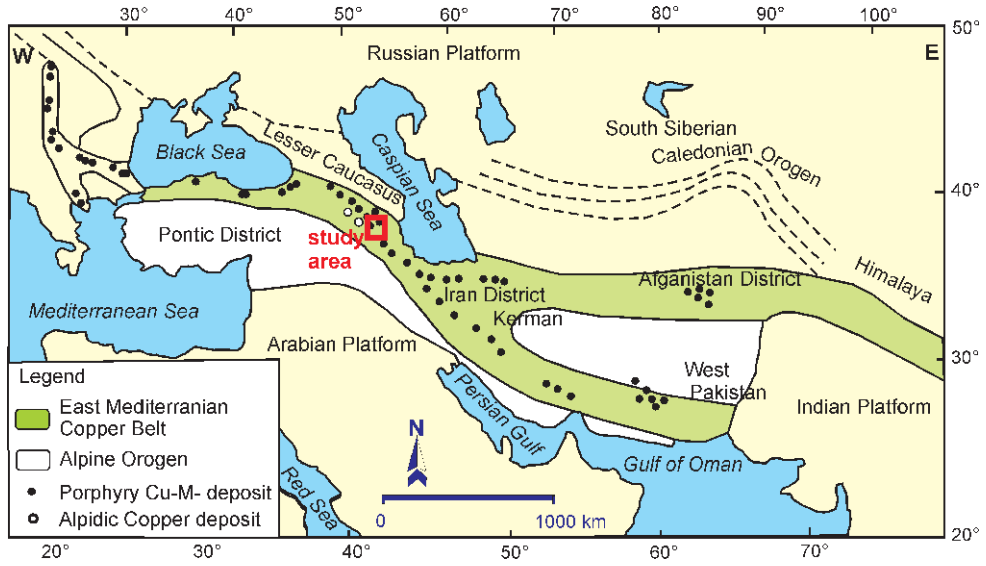

Fig. 1. Map showing the Eastern Mediterranean Iranian–Alpian Copper-Molybdenum belt and the area studied (Modified after Superceanu 1971).

than 100 samples were collected from different rock types and locations. Some representative samples were thin and polished-sectioned and examined microscopically. Electron probe micro-analysis (EPMA) was used to determine mineral compositions of various skarn minerals like garnet, epidote, pyroxene and actinolite, in the Iranian Mineral Processing Research Center (IMPRC), Karaj town. Selected samples for whole-rock geochemical analysis were pulverized using a shatter box with an iron bowl. These powders were analysed in Activation Laboratories Canada according to their Code 4Litho research and Code 4B1 packages, which combine lithium metaborate/tetraborate fusion major element analysis with a trace element ICP-MS package. Fluid inclusion studies were conducted on more than 50 doubly polished plates using a Leitz 1350 heating stage, a SGE gas flow heating/cooling system based on a U.S. Geological Survey design (Hollister et al. 1981), and a Chaixmeca stage at the Fluid Inclusion Laboratory of the Wadia Institute of Himalayan Geology, Dehra Dun, India, and the Department of Earth Sciences, Indian Institute of Technology, Mumbai, India.

Magmatic activities in the Ahar Region

A belt of skarn porphyry Cu deposits of late Tertiary age extends from the Caucasus Mountains to the Alborz unit in the Azerbaijan region of NW Iran and includes the well-known Sungun, Mazraeh, Anjered porphyry skarn deposits (Mollai 1993). All of these deposits are related to the Cenozoic magmatic activity; the Eocene–Oligocene period can be considered as a metallogenic epoch that formed the Alborz-Azerbaijan magmatic belt. Large Cu-Mo porphyry deposits, Cu skarn occurrences, and Cu-Mo-Au porphyry — vein deposits in this area attest to the economic value and potential of mineralization in this magmatic belt (Jamali et al. 2010).

There are three parallel magmatic arcs in the northwest of Iran, of Cretaceous and Eocene–Miocene to Quaternary ages, trending in a NW–SE direction between the Main Thrust zone in the southwest and the Tabriz Fault in the northeast (Azizi & Moinevaziri 2009). Major tectono-magmatic events in northwestern Iran are the result of geodynamic evolution of Tethys belt that formed between the Arabian and Eurasian plates during the Early Mesozoic to Late Cenozoic orogeny (Aghanabati 1993). Among these magmatic activities in the area of study, the Ahar Batholith and the Sungun porphyry stock are the most important. The host rocks have a calc-alkaline, I-type chemical composition of a continental arc geotectonic setting (Fig. 2). The Ahar batholith, which extends about 30 km E–W and is 3 to 10 km wide from north to south, ranges from granite to granodiorite (Fig. 2). The batholith was responsible for mineralization, skarnification and hornfels at its margins. The granodiorite pluton has been affected by a number of later magmatic activities which include various types of quartz, aplite, and pegmatite veins, hypabyssal and mafic dykes, as well as Quaternary volcanic products. There are more than five volcanic masses belonging to Quaternary episodes within the plutonic body of Oligocene age. These igneous activities do not form a single large central volcano. Two mineralized mafic dykes have been noted in the eastern part of Javanshykh village. Malachite as a secondary mineral is distributed within the main body in different forms (Fig. 3b).

The stock of Oligo-Miocene age, which ranges in composition from quartz monzonite to granite, hosting the Sungun Copper Porphyry deposit (Mehrpartou & Torkian 1994; Hezarkhani et al. 1999; Calagari & Hosseinzadeh 2006a) shows a calc-alkaline, I-type chemical composition of a continental arc geotectonic setting. The stock is located about 100 km NE of Tabriz and 85 km NW of Ahar, crops out over an area of about 1.5 by 2.3 km (Calagari 2004) (Fig. 2), and intruded a series of Eocene arenaceous-argillaceous and Upper Cretaceous carbonate rock sequences. The stock consists of three different intrusive phases: (1) monzonite-quartz monzonite, (2) diorite-granodiorite and (3) andesite and re-

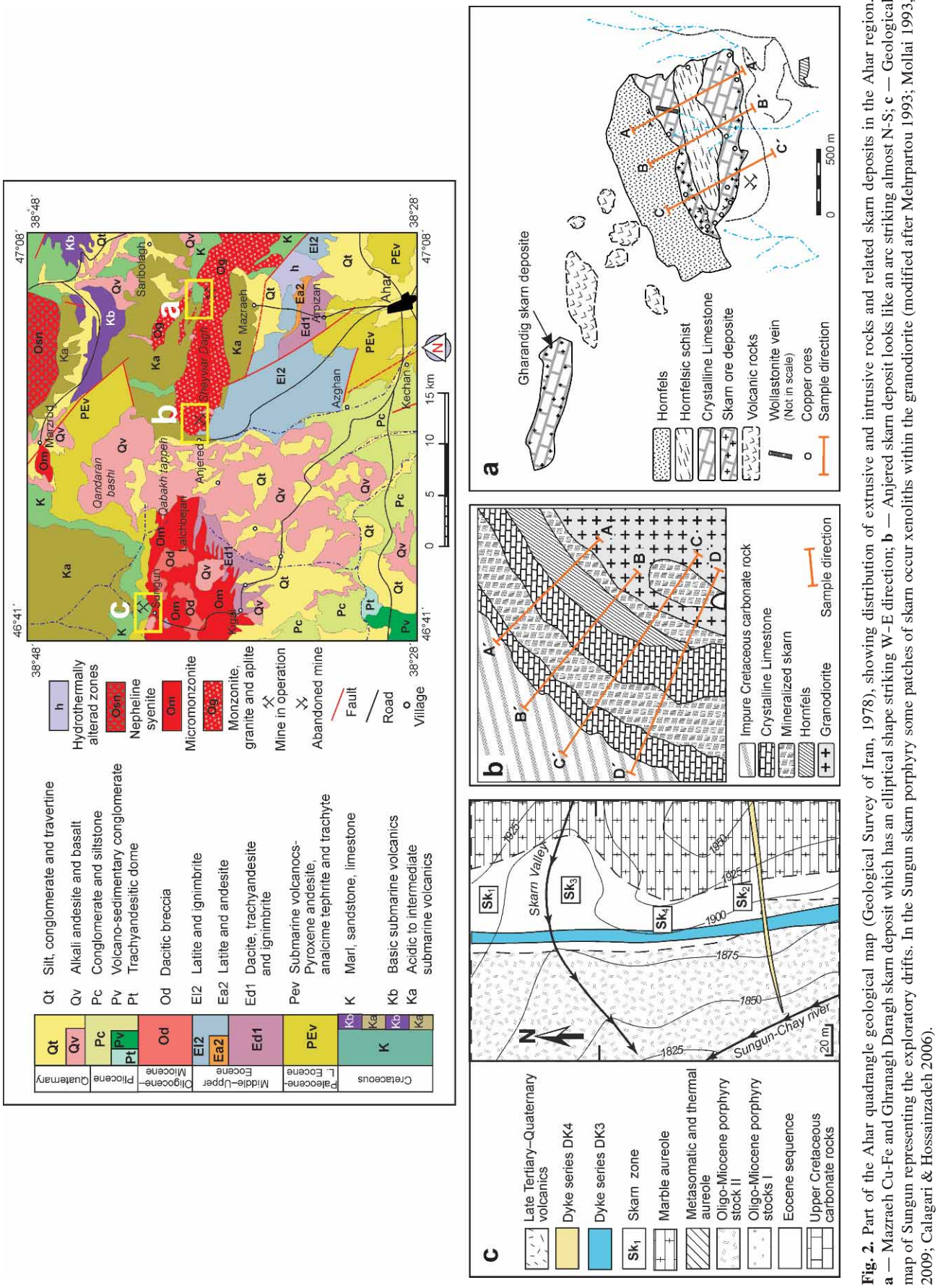

Fig. 2. Part of the Ahar quadrangle geological map (Geological Survey of Iran, 1978), showing distribution of extrusive and intrusive rocks and related skarn deposits in the Ahar region. **a** — Mazraeh Cu-Fe and Ghranagh Daragh skarn deposit which has an elliptical shape striking W-E direction; **b** — Anjered skarn deposit looks like an arc striking almost N-S; **c** — Geological map of Sungun representing the exploratory drifts. In the Sungun skarn porphyry some patches of skarn occur xenoliths within the granodiorite (modified after Mehrpartou 1993; Mollai 1993, 2009; Calagari & Hossainzadeh 2006).

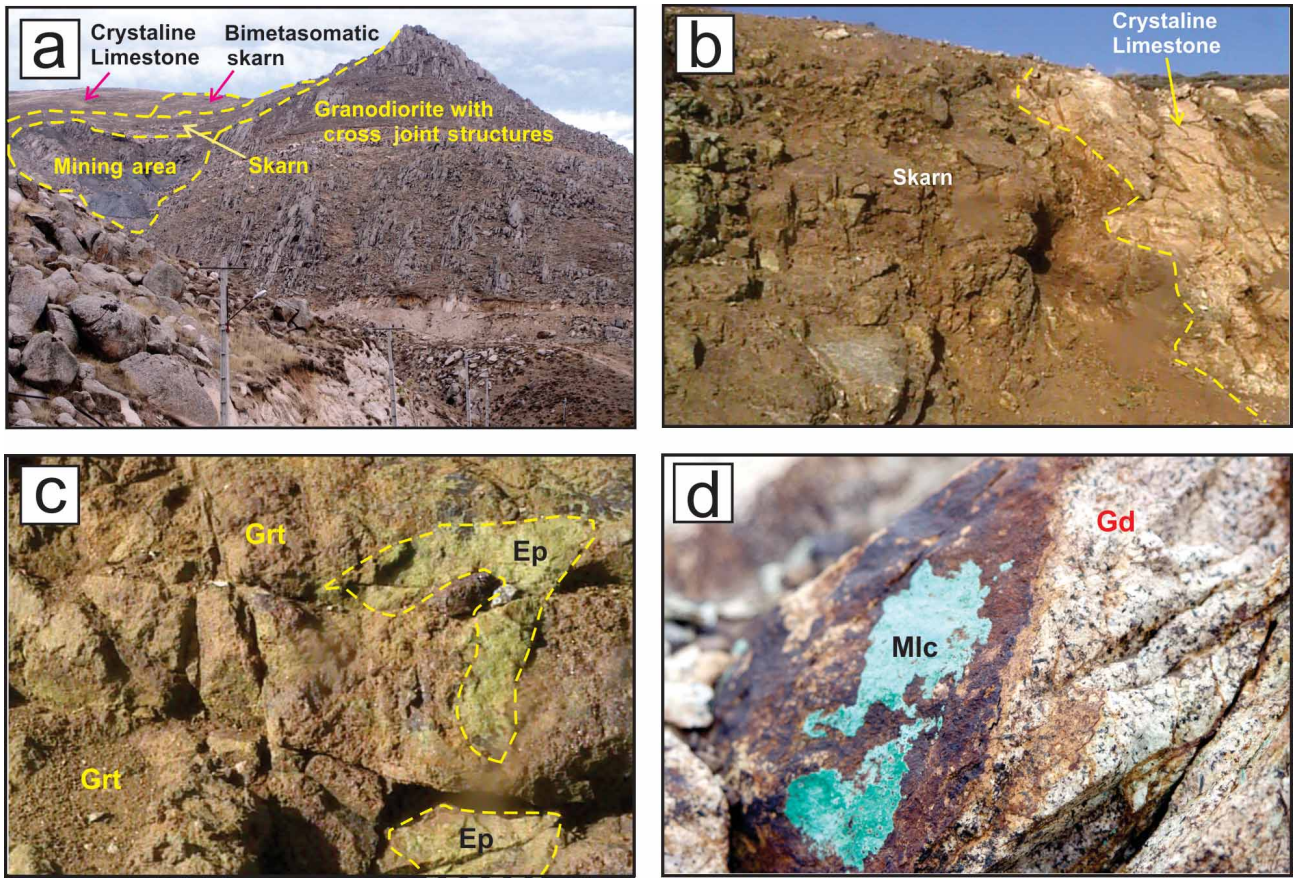

Fig. 3. Field photographs showing various rock types in the studied area. Intense modification of country rocks is unrecognizable and sharp contact between skarn and crystalline limestone is common in the Ahar region skarn deposit. **a** — Morphology and cross joint structure of granodiorite, position of skarn deposit, crystalline limestone and Bimetasomatic zone in the Mazraeh Cu-Fe skarn deposit (Camera towards NE); **b** — Oxide and malachite (Mlc) formation within the Ahar granodiorite (Gd); **c** — Anjered skarn deposit showing intense modification of host rocks leading to the formation of exoskarn, with sharp contact between skarns and crystalline limestone (Camera towards NW); **d** — Intense modification of host rocks in the Anjered skarn deposit — growth of coarse grains of green epidote (Ep) and brown coloured garnet (Grt).

lated dykes (Etminan 1978; Mehrpartou & Torkian 1994; Hezarkhani & Williams-Jones 1998; Hezarkhani et al. 1999; Karimzadeh Somarin 2004). The diorite-granodiorite is volumetrically the next most important and hosts most of the mineralization. These intrusive phases are cut by monzonite and andesitic dykes, which in the northern and eastern parts of the Sungun stock are locally mineralized. A comparison of these granodioritic rocks related to the Cu-Fe skarn deposits in the north west of Iran with other granodioritic rocks related to Cu, Fe and Cu-Au skarn deposits in the world (Table 1) indicates that most of them have similar mineralogy and chemical composition with orthomagmatic mineralization. The host rocks show a calc-alkaline, I-type chemical composition of a continental arc geotectonic setting.

Geology of skarn deposits

Skarn ore deposits in the Alborz range of northwest Iran formed at or near the contact of Tertiary (Oligo-Miocene) magmatic bodies with Cretaceous impure limestone. Both endoskarn and exoskarn are developed along the contact with ore skarn in between as a discontinuous belt. At the contact between the Ahar granodiorite and Cretaceous carbonate rocks the earliest changes observed in the protolith involve recrystallization to coarse grained crystalline marble and fine-grained, dark grey-green hornfels, with an assemblage of clinopyroxene-feldspar-quartz. The endoskarns are very restricted to narrow strips, developed towards the plutonic rocks. Endoskarn indicates the fluid flowed through the plutonic rocks and replaced aluminosilicate minerals along the contact with Cretaceous carbonate rock. Most of the endoskarns are very thin with maximum thickness of a few meters, whereas the thickness of endoskarn in the Elebi District reaches up to 50 m. In general, all of these skarn deposits, irrespective of their size and shape, have sharp contacts with both the intrusive body as well as the crystalline limestone and have almost the same mineral composition. Among these skarn deposits the most important are (1) Mazraeh Cu-Fe skarn deposit, (2) Anjerd Cu skarn and (3) Sungun Cu-Mo skarn, (Fig. 2). These skarn deposits in the field and hand specimens show various colours from dark brown to greenish depending on their mineralogy. In most places the metasomatism is so intense that the original

Table 1: Comparison of granodiorite related to the Cu-Mo and Cu-Fe skarn deposits of the Ahar region NW Iran, with the granodiorite related to the skarn deposit of other parts of the world.

Deposit	Size(t)	Grade	Metal	Associated igneous rocks	Host rock	Early minerals	Late minerals	Ore minerals	Reference
Mazraeh Cu, Fe	40.000 t	1.2 % Cu and Fe	Cu and Fe	Granodiorite	Impure carbonate and granodiorite	Pyroxene, garnet	Epidote, chlorite, calcite, sericite	Cp, py, mt and hem	Mollai 1993, 2009
Sungun	1bt	0.62 % Cu and 0.01 % Mo	Cu and Mo	Diorite/ granodiorite to quartz-monzonite	granodiorite to monzonite and impure carbonate rocks	Pyroxene, garnet	Epidote, chlorite, calcite, sericite	Cp, mo, py, bor and chal	Etminan 2012
Anjerd	20,000 t	0.8 % Cu	Cu	Granodiorite quartz-monzonite	granodioritic and impure carbonate rocks	Pyroxene, garnet	Actinolite, epidote, chlorite, calcite and quartz	Cp, py, mt	Mollai 2009/unpubl. proj.
Daiquiri, Cuba	100 m.t.	Mainly Fe	Fe	Diorite, Limestone	Diorite, limestone limestone blocks	Pyroxene, garnet	Ep, cal, qz	Mt, hem, (py, cp,)	Lindgren & Ross 1916
Peschansk Ural	173 m.t.	50 % Fe;	Fe ,Cu	Diorite	Tuff, sandstone, andesite, limestone	Garnet, pyroxene	Epidote, chlorite, calcite, diopside, sericite	Magnetite, minor chalcopyrite	Sokolov & Grigorev 1977
Bagirkac	250,000 t	7 % Pb	Pb, Zn, Cu	Granite, granodiorite of Eybek Pluton	Skarn after calcareous, marble bearing schist	Wo, ad-gr, di-hd, scp	Cal, tr	Sp, cp, gn, hem, py	Dora 1971
Shinyama japan	10,000,000 t	Fe 30 %–35 % Fe Cu ore 30–35 % Cu 1 %	Fe-cp, py, sph	granodiorite of Samli Pluton	Basaltic andesite, limestone	Ad-gr, di-hd,	Act, qz, tourmaline, tr, cal, ep	Mt, cp, cubanite, pyrrh, sph,	Tsusue 1961; Kaneda et al. 1978
Bingham Utah	100,000,000 t	3.2% Cu, 0–03% Mo	Fe	Monzonite to Quartz monzonite	Calc-silicate hornfels after metamorphic rocks	Ad-gr, di-hd	Ep, cal, amp	Cp, py, born,	Atkinson & Einaudi 1978; Sweeney 1980
Evciler Kazdag	no estimate	Au (up to 14 ppm) in pyrrhotite	Fe	Granodiorite to quartz diorite of Evciler Pluton	Hornfels after metamorphic rocks, skarn after limestone	Ad,gr, di-hd, scp,py	Ep ,cal, amp, chl, qz	Po, py, cp	Ozturk et al. 2005; Ozturk et al. 2008
Shinyama mine, Japan	>10 m.t.	30–35% Fe, 0.1% Cu	Fe–Cu	Diorite-granodiorite dykes, stock	Basaltic andesite, dacite, Permian black slate, limestone	Gr, di, fer	Epidote, amphibole, actinolite, quartz, magnetite; in marble: pageite, tourmaline, magnetite, calcite, phlogopite	Mt; minor cp, cub, pyrrh, sph, trace pentlandite, valleriite, arsenopyrite, comackinawite	Tsusue 1961; Kaneda et al. 1978
Ayazmant Ayvalik Turkey	5,750,000 t	46% Fe and 0.6% Cu	Fe–Cu	Granodioritic to monzodioritic porphyries of Kozak Plutonic Complex	Hornfels after regional metamorphic rocks with carbonate lenses and intercalations, skarn after limestone lenses	Di, ad-gr, scp	Ep, amp, py, or, chl, cal, qz	Mt, cp, py, bn, mo, go, hem, po, gn, sp, various Au-Ag-Te-Se minerals	Tolga Oyman 2010

character of the Cretaceous carbonate rocks as well as the igneous rocks are unrecognizable. The skarn deposit in the area reveals that after a hot gaseous stage, there was hydrothermal activity which resulted in the alteration of igneous rocks.

The structural set up of the Mazraeh mine is an elliptical shaped mega enclave of meta-sedimentary rocks within the Mazraeh granodiorite, with the 1.5 km long major axis striking E–W and the 1.0 km long minor axis running in N–S

direction (Fig. 2a). The southern contact between the granodiorite and crystalline limestone is steeply dipping (60° to 70°S) and is sub-concordant, transecting the limestone beds (striking E-W, dipping S). The width of skarn here ranges from 2 to 25 m, except where a granodiorite tongue cuts across the limestone and the skarn width is 50 m. Exoskarn is the principal skarn zone enclosed by the marmorized- and endo-skarn zones. A vein of wollastonite with a NE-SW direction and thickness of about 50 cm, occurs in the north east of the mine within the crystalline limestone. Fig. 2 shows the zonal arrangement of skarn deposits (Mollai 1993). The mine is now (summer 2012) abandoned.

The Anjered Cu skarn deposit is located at the western limit of the Ahar batholith (Fig. 2). The structural set up of the Anjered skarn deposit is a semi elliptical shape, with 1 km long major axis striking almost N–S along the contact of igneous rocks and 500 m thickness of minor axis running in a W–E direction (Fig. 2b). In most of the places near the contact with granodiorite, the skarn is covered by loose eroded material. Therefore the size of the Anjered skarn in such places may be underestimated. The remains of old tunnels in the contact between the granodiorite and impure carbonate rocks show that mining activities have been carried out in the past.

The intrusion of Oligo-Miocene porphyry granodiorite of Sungun into the impure limestone of Cretaceous rocks led to the formation of the Cu-Mo skarn deposit, recrystallizing the impure limestone and hornfels in the east Sungun river (Fig. 2c). Skarn-type metasomatic alteration and mineralization occurs along the contact between Upper Cretaceous impure carbonates and an Oligo-Miocene Cu-bearing porphyry stock. The structural set up of Sungun porphyry is a narrow zone with the thickness of 55 m to 60 m. Both endoskarn and exoskarn are developed along the contact. Exoskarn is the principal skarn zone enclosed by marmorized carbonates and skarnoid hornfelses. Petrographic studies in the Sungun area show that the mineralized dikes are mainly andesitic and are related to the diorite-granodiorite intrusive phase, whereas the andesite dykes in Mazraeh are barren. Molybdenum was concentrated at a very early stage in the evolution of the hydrothermal system and copper somewhat later. Four distinct types of hypogene alteration are easily distinguished as follows: 1) Potassic, 2) Potassic-phyllic, 3) Phyllic, 4) Propylitic (Mehrpartou & Torkian 1994). The metamorphic rocks along with bimetasomatic skarns occur in the Mazraeh and Sungun skarn deposits, but this phenomenon was not clearly observed in Anjered. The portion of metamorphic interlayering of bimetasomatized zones varies in thickness from 70 to 120 m in Sungun (Calagari & Hosseinzadeh 2006b) and 50 to about 200 m in the Mazraeh skarn deposit. This zone in both skarn deposits lies between exoskarn and impure Late Cretaceous carbonate rocks. These rocks, in addition to being thermally metamorphosed, have been bimetasomatized and have also produced bimetasomatic skarn (Einaudi et al. 1981). At a relatively long distance from the contact of magma, this heat source caused the development of ne-grained anhydrous calc-silicates (mainly isotropic garnet and pyroxene) within the clay-rich inter-layers in the impure carbonates. Some amounts of hydrous silicates like biotite, amphibole, epidote and chlorite are present; these minerals are the retrograde products. The thickness of these bimetasomatized layers never reaches more than 10 cm. In the north and north east of the Mazraeh skarn deposit, various types of folding are present, which are due to syntectonic conditions in the impure carbonate rocks. In the bimetasomatic skarn, brownish elephant skin structures occur as a result of deep weathering of crystalline limestone leaving residual metasomatized minerals.

Petrography and mineralogy

Petrography and mineralogy of igneous rocks

Texturally the granodiorite is coarse grained and porphyritic. Its modal composition ranges are 6–15 % quartz, 24–43 % plagioclase, 20–48 % K-feldspar, 0–10 % hornblende, 0–5 % biotite, and 0–3 % each of apatite, sphene and magnetite. Micro diorite rock contains large isolated crystals (phenocrysts) of plagioclase and hornblende in a mass of fine textured crystals in which they develop a porphyritic texture (Fig. 4a–d). Some feldspars display poikilitic textures and perthitic and myrmekitic intergrowths were recognized in some samples. Alkali feldspar in places jackets the plagioclase laths, which is indicative of their order of crystallization. Veins of both quartz and calcite cut the granodiorite. According to XRD and microprobe analyses, the plagioclase is the most abundant mineral and ranges from albite to oligoclase. K-feldspar has been confirmed as orthoclase and plagioclase crystals are lath-shaped, unzoned or zoned with both albite-type and pericline twinning. Plagioclase shows a paragenetic relationship with sphene. Feldspar minerals are partially to entirely altered to sericite, and biotite has changed to chlorite, muscovite and opaque minerals. (Fig. 4b,c). Porphyritic texture indicates that a magma has gone through a two stage cooling process. Pyrite and chalcopyrite are the most abundant sulphide minerals present in the porphyritic stock of Sungun. The quartz grains are present in varying sizes, some with inclusions of feldspar, biotite, apatite, sphene and magnetite. Sphene is a very common accessory mineral, occurring as anhedral to well developed euhedral lozenge-shaped grains with high relief (Fig. 4d). They are associated with epidote, biotite, rutile, and opaque minerals.

Thin section studies of samples from the Sungun porphyry host rocks show porphyritic texture, containing phenocrysts of plagioclase, K-feldspar, quartz and biotite. In some altered rocks feldspar minerals are partially to entirely altered to sericite, and biotite has changed to chlorite, muscovite and relics of opaque minerals. Thin section studies show two types of opaque mineral, the first type is primary mineral and the second one is the altered product of mafic minerals. Most of opaque minerals in Sungun porphyry are sulphide minerals (pyrite, chalcopyrite, molybdenite, blende and galena) whereas the opaque minerals in Mazraeh granodiorite are mainly magnetite. The mineralized dikes are mainly andesitic and are related to the diorite-granodiorite intrusive phase. These deposits reveal that after a hot gaseous stage, there was hydrothermal activity which resulted in the alteration of igneous rocks.

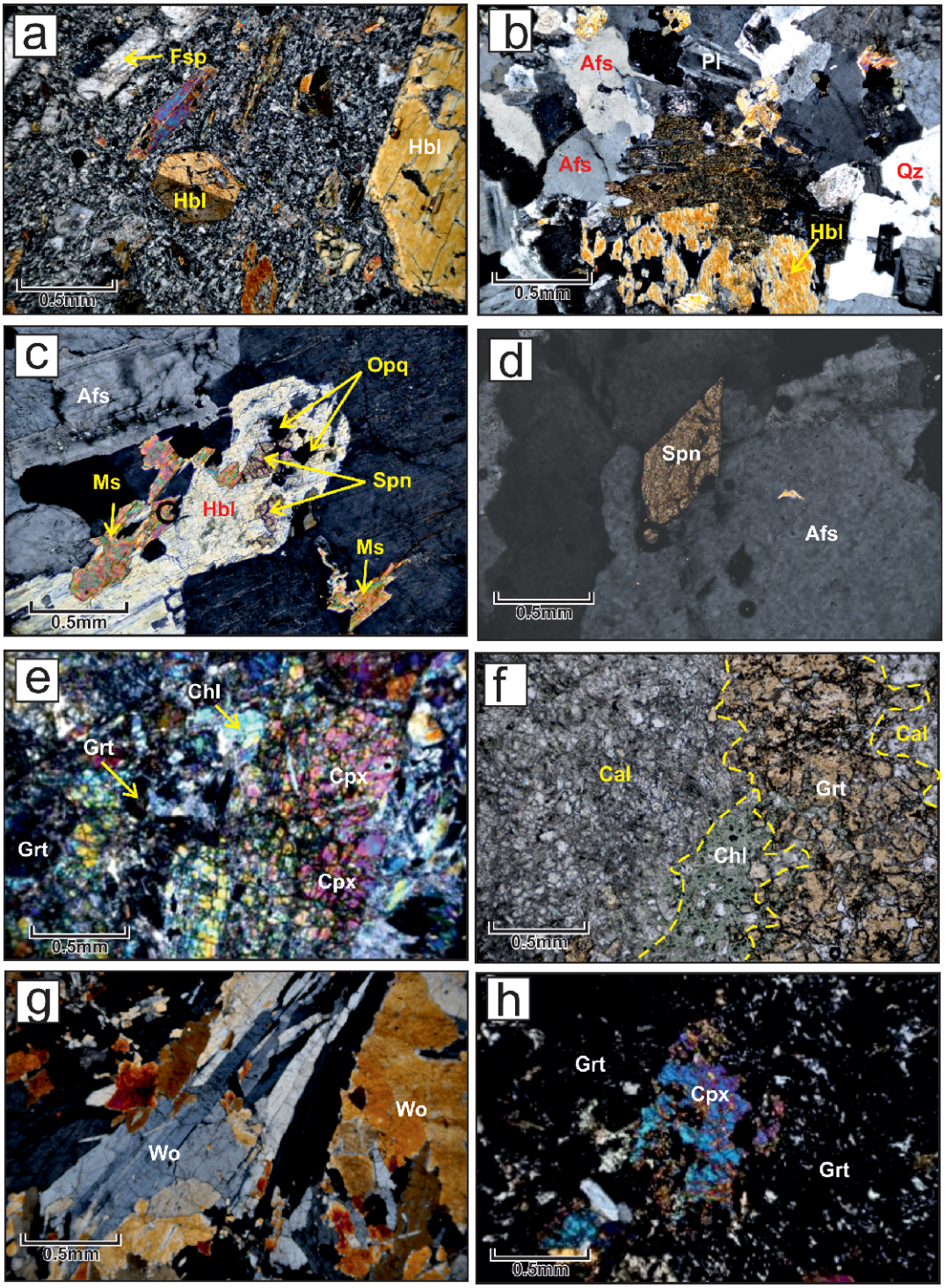

Fig. 4. Microphotographs of thin sections for various rocks of the studied area. **a** — Micro-diorite with porphyritic texture, groundmass of orthoclase, plagioclase and some grains of quartz and well-developed large grains of hornblende and bladed plagioclase. Some of the hornblende shows twinning; **b** — Granodiorite with subhedral to anhedral large grains of hornblende along with plagioclase and alkali feldspars and a few grains of quartz. Felsic minerals do not show alteration, however, hornblendes are altered; **c** — Granodiorite in which hornblende is partially included within alkali feldspar, with sphene and magnetite as inclusions within the hornblende. Secondary muscovite replaces alkali feldspar and hornblende; **d** — Rock contains mainly large grains of alkali feldspar and sphene along with some quartz. Well developed sphene grain is euhedral, surrounded by alkali feldspar (Afs); **e** — Pyroxene-garnet exoskarn: garnet is medium grained and isotropic, whereas pyroxene shows well developed grains with porphyroblastic texture and minor alteration to actinolite; **f** — Bimetasomatic skarn under ppl showing interlayering of garnet skarn with calcite as well as alteration of garnet (Grt) to chlorite (Chl); **g** — Coarse-grained wollastonite vein occurring within the crystalline limestone in the northern part of the Mazraeh Cu-Fe mine; **h** — Coarse-grained altered clinopyroxene within isotropic garnet indicates an earlier formation of the pyroxene.

Skarn mineralogy

In general the dominant calc silicate (skarn) minerals in the area are garnet, calcite, pyroxene, actinolite and epidote, which are accompanied by quartz, feldspar, minor vesuvianite and hornblende. These skarn deposits can be petrologically classified into: (I) Exoskarn, (II) Endoskarn and (III) Ore skarn. Each of the skarn types can be further divided on the basis of their mineral assemblage. In general, the rocks in this zone contain principally ne-grained granoblastic calcite (50–98 %), garnet (0–35 %), pyroxene (0–10 %), epidote (0–5 %), chlorite (0–2 %), clays (1–3 %), and sulphides (<0.5 %) (Calagari & Hosseinzadeh 2006a).

(I) Exoskarn: The exoskarn is developed within the country rock and the bimetasomatic skarn (Einaudi et al. 1981; Einaudi & Burt 1982; Kwak & Kwak 1987). The alteration of the host rock (impure carbonate and igneous rocks) in the Ahar region is marked by the formation of coarsely crystalline skarn bands due to the introduction of Si-, Al-, Fe-, and Mg-rich fluids into the host rock. Metasomatism of carbonate in the Ahar region produced andradite- grossular/pyroxene exoskarn, as components of the prograde assemblage, and epidote, tremolite/actinolite, chlorite and/or calcite and quartz as components of the retrograde mineral assemblage with few grains of vesuvianite (Fig. 4a,b and c). The skarn shows porphyroblastic, poikiloblastic brecciation, overprinting and in some cases cataclastic textures. Pyroxene shows porphyroblastic texture with alteration to actinolite (Fig. 4e). There are at least two generations for most of the minerals especially garnet, quartz, calcite, chlorite, magnetite and chalcopyrite. For example, garnet occurs at least in three generations with different geological and optical properties. Garnets range in size from 0.1 mm up to 4 cm in diameter, showing fine to coarse grains of isotropic and concentric, oscillatory zoning of anisotropic garnet (Fig. 4h). Most of the pyroxene minerals were replaced by garnet. Idiomorphic, twinned epidote occurs in exoskarn as well as in endoskarn (Fig. 5e,f). Very well developed, coarse grains of wollastonite occurring as a vein within the crystalline limestone in the north-east of the Mazraeh skarn deposit show porphyryblastic texture (Fig. 4g). Actinolite mineral, which is the altered product of pyroxene and garnet minerals, is more predominant in the Anjered skarn in comparison with other skarn deposits in the area. The alteration has started from the borders of minerals, with the remnants of pyroxene and garnet observed within the actinolite.

(II) Endoskarn: Along the contact with the exoskarn, replacement of granodiorite by massive epidote and minor garnet-pyroxene over widths of centimeters to 0.5 m may result in complete destruction of the original igneous texture and mineralogy. This is the evidence of progressive addition of calcium from country rocks into the intrusive magma and loss of Al, Si and also Na. This skarn comprises: plagioclase, alkali feldspar, magnetite, epidote, biotite, garnet, pyroxene, hornblende, actinolite, sericite, siderite and opaque minerals (Fig. 5a and b). As in the exoskarn, two types of garnets are observed in the endoskarns: subhedral to anhedral, isotropic garnets and larger, well developed, oscillatory-zoned anisotropic garnets. Pyroxene is generally subhedral to euhedral, and hedenbergitic to diopsidic in composition. Endoskarn formation began with epidotization, and was coincident with sericitization during metasomatic reactions. This zone consists of medium to coarse and well developed-grained epidote accompanied by interstitial quartz, pyrite, chalcopyrite, and iron oxide (Fig. 5e and f). Where the alteration has changed the endoskarn, the remnants of garnet and pyroxene are observed within the hydrothermal product minerals (Fig. 5c and d). Farther into the granite, endoskarns occur only as disseminated epidote skarns, and are enriched in garnet towards the impure carbonate rock (Fig. 4f). The garnet-rich skarn predominantly comprises exoskarn. However, garnet locally developed by dissolution and replacement of primary igneous minerals, particularly feldspar, in the granodiorite; such garnet is rich in grossularite. Sericitization and carbonitization of igneous rocks in the retrograde stage of skarn formation lead to the formation of typical endoskarn of sericite-siderite, feldspar, and actinolite-epidote. Epidote skarn is the only predominant Al-rich skarn in the study areas, and it reaches up to 80 % and 65 % in Sungun and Mazraeh skarn deposits respectively (Mollai 1993; Calagari & Hosseinzadeh 2006a), whereas in Anjerd skarn actinolite is more abundant.

(III) Ore skarn: The early-formed calc-silicate minerals were later texturally replaced by oxides (magnetite, hematite), followed by sulphides (chalcopyrite, pyrite, covellite, bornite, galena, sphalerite and molybdenite), hydro silicate (actinolite, epidote, chlorite and sericite) and carbonates (calcite, ankerite and siderite). Oxides in the Cu Sungun and Anjered skarn deposits are not predominant minerals, in contrast to the Cu-Fe Mazraeh skarn deposit.

The ore-forming fluids were initially thought to be of magmatic origin only. Sulphur and oxygen are among the most important volatiles which play a significant role in the formation of hydrothennal sulphide and oxide deposits (Schwartz 1950). Magnetite shows replacement texture, including relicts of replaced minerals like garnet, calcite and sometimes feldspar. In addition magnetite is intercrystalline as well as intracrystalline with garnet. Garnet usually shows corrosion boundaries with magnetite depicting reaction. In places, magnetite shows cataclastic texture with numerous fractures, which are filled by third generation minerals like quartz, calcite and sometimes chalcopyrite. In such conditions we can see various veins of magnetite, sulphide and quartz (Fig. 6a). The martitization of magnetite is quite common, and is due to the changes of oxygen fugacity (Fig. 6b). It occur as lamellar plates along octahedral planes, fractures, zonal growth planes and outer margins, where hematite is comparatively thicker (Mollai et al. 2009). Where the degree of martitization is extensive, magnetite occurs as relicts.

Chalcopyrite is the most common sulphide in these skarn deposits, along with bornite, and molybdenite in the Sungun deposit. In the Sungun porphyry, sulphides occurring within the feldspar altered zone are disseminated, while in the phyllic zone they occur as veins. The argillic zone has low grade disseminated ores. More specifically the metallic ores present, in decreasing order of abundance, are: chalcopyrite, pyrite, bornite, molybdenite and pyrrhotite, with minor cubanite (Mehrpartou 1993; Mollai 1993; Calagari & Hosseinzadeh 2006a). Chalcopyrite associates closely with bornite and also partially to fully replaces magnetite, sometimes re-

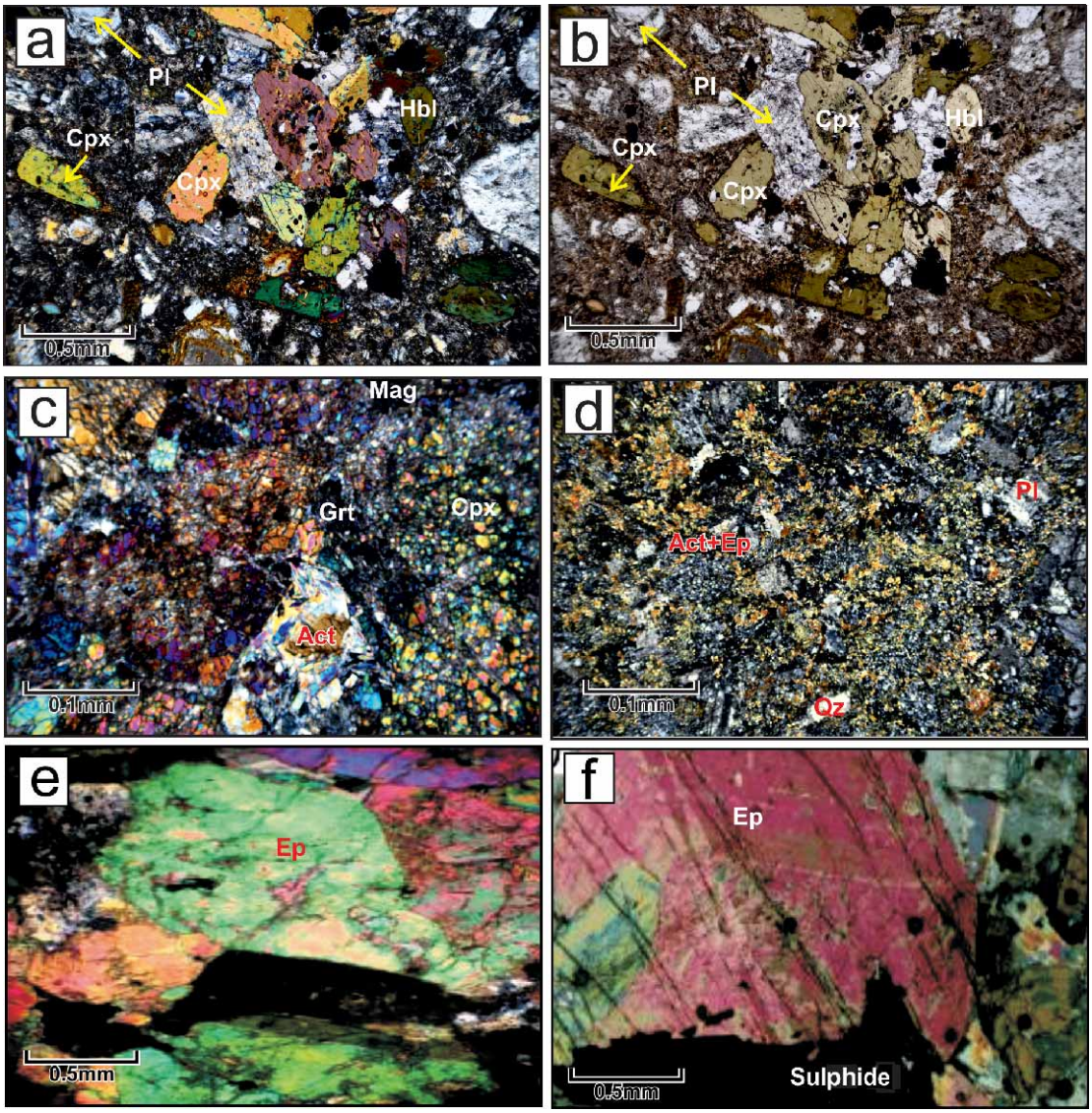

Fig. 5. Microphotographs showing the mineralogy and textures of endoskarn. **a** — xpl and **b** — ppl — showing replacement of primary igneous minerals like plagioclase and feldspar by pyroxene and some garnet. Coarse and euhedral to subhedral porphyritic pyroxene overgrows the igneous minerals. Magnetite is of two types: primary and secondary, the latter due to alteration of pyroxene. The groundmass is mainly very fine grained minerals; **c** — Pyroxene-garnet-actinolite endoskarn with porphyroblastic texture (xpl); **d** — Fine grains of epidote, actinolite and opaque minerals overgrown on igneous mineral during retrograde skarn formation, leading to the formation of feldspar-epidote-actinolite endoskarn (xpl); **e, f** — Epidote sulphide skarn, with chlorite and quartz formed by alteration of anhydrous minerals like garnet and pyroxene. (Epidote with well developed zoning and twinning along with porphyroblastic texture showing its replacement by sulphide ores.)

placing intensively the host rock as well as silicate gangue minerals (Fig. 6c and d). Sulphide ores in the Mazraeh and Anjered deposits occur within the skarn zone only, but the distribution of sulphide ore in Ghranigh Deragh on the northern slope of the Ahar granodiorite is like at Sungun, namely disseminated within porphyritic granodiorite. Quartz is coeval with the sulphides as veinlets cutting magnetite. Sulphide bearing quartz veins, which are called mineralized quartz veins, are very common within the magnetite. These indicate that sulphide ores postdate the iron ores and may also occur as intergranular fillings (Fig. 6a). Chalcopyrite has an affinity with magnetite and occurs together with epidote (Fig. 5e and f).

Mineral chemistry of skarn minerals

Garnet

According to EPMA data the andradite mole fraction in the garnet ranges from 30–99 %, followed by grossularite (0–57 %), and pyralspite (0–13 %) (Table 2). The composition of garnet appears to be controlled by the chemistry of the replaced mineral: garnet replacing plagioclase is richer in grossularite and that replacing pyroxene and calcite is richer in andradite. Within the ugrandite area, the pyralspite content increases with increasing substitution of Mg and Mn for Ca and the grossular content increases with increasing sub-

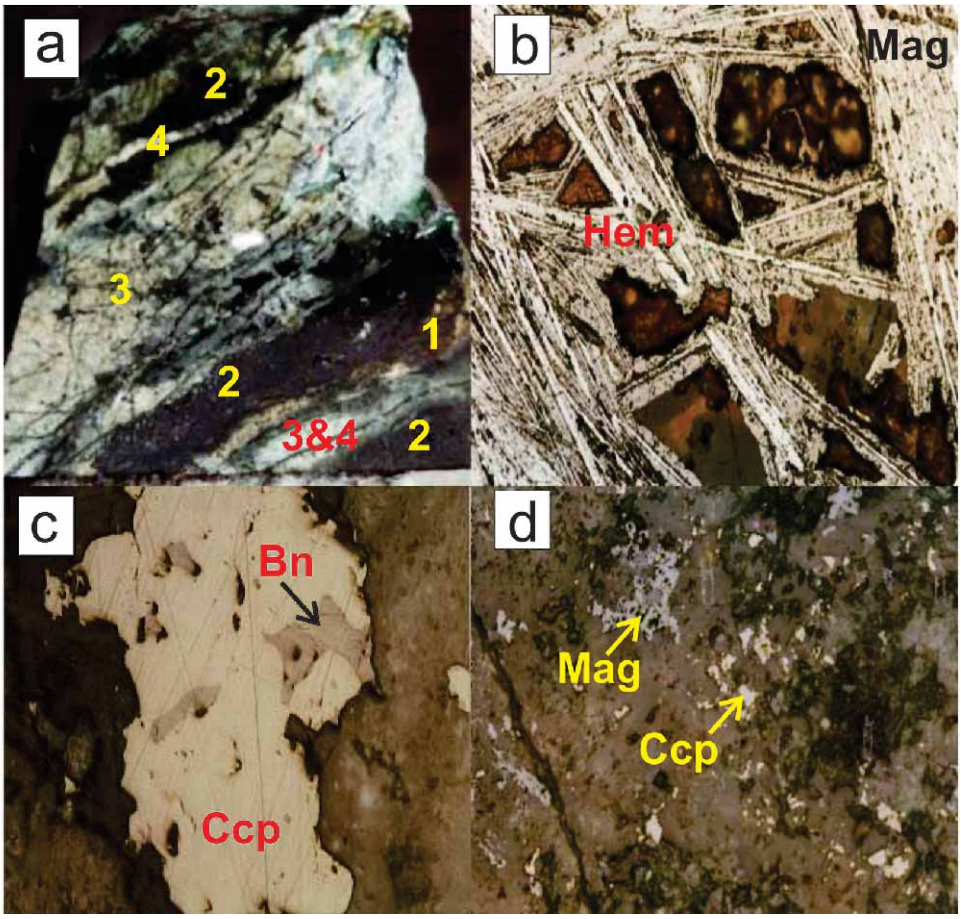

Fig. 6. a — shows intense and multiple replacement hand spacemen of skarn and formation of ore skarn. No. 1 — shows the remnant of brown garnet after replacement by magnetite. No. 2 — shows magnetite veins replacing garnet. No. 3 — shows an intense replacement of early rocks by sulfide and quartz. No. 4 — mineralized quartz veins belonging to the 4th stage of alteration or hydrothermal activity; **b** — is a microphotograph of a polished section showing replacement of radial magnetite by hematite due to martitization. Blades consist of martite crystals (5–20 mm) which represent the hematitization of euhedral magnetite. The replacement process includes an initial iron atom diffusion through the oxygen framework leading to maghemite, followed by inversion of maghemite to hematite and development of distorted octahedrons; **c** — microphotograph of polished section shows replacement of magnetite and anhydrous minerals by patches of chalcopyrite along with bornite; **d** — microphotograph of polished section shows replacement of silicate minerals by magnetite and chalcopyrite.

Table 2: Representative electron microprobe analyses of garnet in the Ahar region skarn deposits, NW Iran (in weight percent, 12 oxygen basis).

Samples	MZ551	MZ552	MZ553	MZ8121	MZ8122	MZ8123	311	312	841	842
SiO_2	35.37	35.32	35.58	36.75	35.54	36.28	33.95	34.04	39.15	33.92
Al_2O_3	7.37	6.50	7.09	15.66	9.24	11.55	0.88	0.02	0.04	0.99
Fe_2O_3	21.29	22.21	20.66	10.69	20.38	16.27	29.84	31.26	31.09	30.26
MgO	0.24	0.20	0.23	0.18	0.19	0.25	0.03	0.04	0.00	0.00
MnO	0.67	0.76	0.61	3.11	3.18	3.48	0.43	0.32	0.32	0.40
CaO	35.04	35.05	35.83	33.26	31.47	32.08	34.87	34.61	34.40	34.48
Total	99.93	100.00	100.00	99.66	100.00	100.00	100.00	100.29	100.29	99.99
Si	2.90	2.91	2.94	2.86	2.85	2.93	2.97	2.89	2.92	2.89
Al	0.71	0.63	0.69	1.44	0.87	1.10	0.09	0.02	0.00	0.09
Fe	1.31	1.38	1.28	0.63	1.23	0.98	1.85	1.99	2.00	1.94
Mg	0.03	0.02	0.03	0.21	0.02	0.03	0.04	0.00	0.00	0.00
Mn	0.05	0.05	0.04	0.20	0.22	0.24	0.03	0.02	0.02	0.03
Ca	3.08	3.09	3.11	2.77	2.70	2.76	3.08	3.14	0.15	3.15
Total	8.07	7.08	8.08	8.11	7.89	8.03	8.06	8.06	8.08	8.10
Andra	0.67	0.71	0.65	0.30	0.60	0.46	0.96	99.68	0.99	0.96
Gross	0.31	0.27	0.33	0.57	0.32	0.45	0.02	0.00	0.00	0.03
Pyrope	0.02	0.02	0.02	0.13	0.08	0.09	0.02	0.01	0.01	0.01

stitution of $A1^{+3}$ for Fe^{+3}. In the veins the major cations are Ca^{+2} and Fe^{+3} and the andradite component predominates (>99 %) (Table 3). A notable feature of this vein garnet is the excess of Ca, which is due to the deficiency in Si solid solution (Table 3). The Ayazmant Fe-Cu skarn of Turkey and Kamaish Fe skarn of Japan are richer in grossularite in comparison with the Ahar skarn deposits (Fig. 7). Garnet with 30 to 99 % mole fraction of andradite shows mixed optical properties in the main garnet mass. There is no appreciable change in chemistry except antipathetic behaviour of Al and Fe which could lead to zoning in garnets. The Al-Fe variation could be due to local fluctuations in temperature

Table 3: Representative electron microprobe analyses of vein garnet in the northeast Mazraeh Cu-Fe skarn deposit, NW Iran (in weight percent, 12 oxygen basis).

Oxide/samples	Hyv1	Hyv2	Hyv3	Hyv4	Hyv6	Hyv8
SiO_2	33.54	33.75	33.79	33.73	33.59	33.8
Al_2O_3	0.21	1.34	0.49	0.2	0.75	1.55
Fe_2O_3	31.27	29.93	31.12	31.1	30.57	29.22
MgO	0.03	0.00	0.00	0.00	0.00	0.00
MnO	0.55	0.41	0.60	0.54	0.49	0.5
CaO	34.4	34.56	34.01	34.43	34.21	34.90
Total	99.99	99.99	100.00	100.4	99.61	99.66
Si	2.87	2.87	2.88	2.87	2.88	2.88
Al	0.02	0.13	0.05	0.02	0.02	0.16
Fe	2.16	1.92	2.00	2.02	1.97	1.87
Mg	0.002	0.0	0.0	0.0	0.0	0.0
Mn	0.04	0.03	0.04	0.04	0.04	0.35
Ca	3.16	3.15	3.11	3.17	3.14	3.18
Total	8.19	8.10	8.09	8.12	8.04	8.11

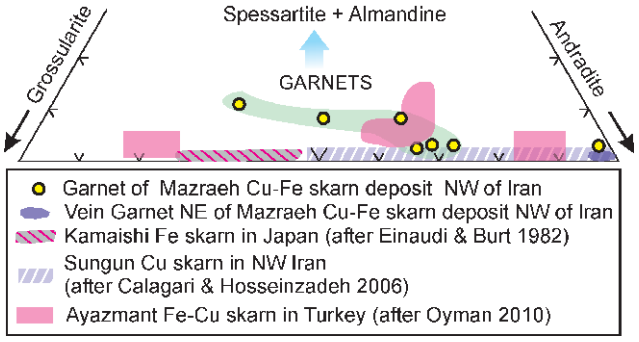

Fig. 7. Ternary plot of garnet composition from the Ahar region in comparison with skarn deposits in other parts of the world.

(Rose & Burt 1979). Optical anisotropy in garnet is due to their departure from the cubic symmetry, as a result of partial replacement of (SiO_2) by (OH) to form hydrogarnet. Rose & Burt (1979) suggested that anisotropic garnet will form due to fluctuation in fluid composition resulting from variable mixture with meteoric water. Zoned garnets from skarn deposits of the Ahar region do not show a systematic compositional variation from the core to the rim of the crystal.

Epidote is one of the important products of hydrothermal fluid that was rich in Al. This Al-rich fluid may have played an important role in carrying sulphide ore solution. Fe^{+3} replacing Al ranges from 71–95 mol % (Table 4). The Mn^{+3} in the epidote ranges between 0.7 and 5.35 mol % piedmontite, whereas the epidote in the Ayazmant Fe-Cu skarn deposit in Turkey (Oyman 2010) is Fe-rich with Fe/(Fe + Al) ratios varying between 0.20 and 0.29. At Ayazmant, epidote resulting from late replacement of grossular-rich garnet shows a higher Fe/(Fe + Al) ratio (mean 0.28) than that which replaces actinolite-magnetite skarn with a mean value of 0.24. During retrograde stages most of the anhydrous calc-silicate minerals like garnet and pyroxene were replaced by a series of hydrous calc-silicates (epidote, tremolite-actinolite), sulphides (pyrite, chalcopyrite, galena, sphalerite and bornite), as well as oxides and carbonates (calcite, ankerite). Processes such as hydrolysis, carbonation and sulphidation, due to relatively low temperature hydrothermal fluids, were responsible for

Table 4: Representative electron microprobe analyses of epidote from the Ahar region skarn deposits, NW Iran (in weight percent, 13 oxygen basis).

Oxide/Samples	Mz332	Mz333	Mz337
SiO_2	37.41	37.8	37.05
Al_2O_3	21.280	22.27	20.45
Fe_2O_3	14.84	13.93	14.99
MgO	0.01	0.03	0.03
MnO	1.15	0.2	0.09
CaO	21.98	23.14	23.42
TiO_2	0.20	0.02	0.35
Cr_2O_3	0.00	0.02	0.0
Ni	0.00	0.0	0.0
F	0.00	0.28	0.24
Tota1	96.05	97.57	96.42
Si	3.15	3.16	3.16
Al	2.2	2.2	2.05
Fe^{+3}	0.88	0.87	0.95
Mg	0.00	0.0	0.0
Mn	0.05	0.01	0.02
Ca	1.96	2.06	2.14
Ti	0.01	0.0	0.01
Total	8.25	8.39	8.31

the formation of these mineral assemblages. A local increase in fO_2 may have played an important role in the formation of epidote (Perkins et al. 1986; Berman 1988), according to the equation:

$Ca_3(Al,Fe)_2Si_3O_{12}(garnet) + {}^5/_4O_2 + HCO_3 \Rightarrow Ca_2FeAl_2Si_3O_{12}(OH)(epidote) + CaCo_3 + {}^1/_2Fe_2O_3$.

Pyroxene in Sungun occurs as fine to medium grained anhedral to subhedral crystals showing decussate texture. Chemically the pyroxene belongs to the diopside-hedenbergite series, with 38 mol % Hd/(Hd + Di) and minor Mn. The pyroxene also contains some Mn, ranging from 0.001 to 0.058 mol fraction, hence the other end member of pyroxene is johansenite with a mol fraction of 0.032. In addition, the presence of a 1.45 mol fraction of Al indicates scapolite (meionite) with the formula of $Ca_4Al_6Si_6O_{24}CO_3$. Tremolite in the Sungun porphyry is mainly the alteration product of pyroxene, according to the equation:

$Ca(FeMg)_2Si_2O_6(clinopyroxene) + 2H_2O + 3CO_2 \Rightarrow Ca_2(Mg,Fe)_5Si_8O_{22}(OH)(Tremo\text{-}actinolite) + CaCO_3 + 2SiO_2$.

In contrast, in the Anjerd Cu-skarn and the Mazraeh skarn deposits, tremolite is mainly the alteration product of garnet as well as pyroxene. Moreover tremolite in the Sungun Porphyry and Mazreah is tremo-actinolite in composition, whereas in the Anjerd Cu skarn it is mainly actinolite with very minor amounts of tremolite (Mollaei et al. 2009).

Geochemistry of igneous rocks

For a better understanding of the genetic relation of skarn deposits and magmatic activity one needs to understand the geochemistry and geotectonic setting of magmatic rocks. Table 5 shows the whole rock analysis of igneous rocks in the region.

The igneous rocks range from diorite and monzonite to quartz monzodiorite and monzodiorite, syeno diorite and granite compositions in the SiO_2 versus Na_2O+K_2O diagram (Fig. 8). In the Harker major element diagrams, K_2O and Al_2O_3 increase with increasing SiO_2 whereas Fe_2O_3 and CaO decrease with increasing SiO_2, and Na_2O displays a more erratic distribution (Fig. 9a,b,c and d). In the alkalis versus SiO_2 diagram and in the AFM diagram (Fig. 9e and f), the samples show a typical sub-alkaline and calc-alkaline trend respectively. All the samples plot on the boundary between the calc-alkaline and high-potassium calc-alkaline fields indicating that K_2O enrichment was already important at the beginning of the liquid line of descent. This suggests that the K_2O enrichment is source-inherited.

The Rb vs. Y+Nb (Fig. 9g) and Nb vs. Y (Fig. 9h) discrimination diagrams both show that the igneous rocks have an I-type granite origin. The Rb, Ba, and Sr ternary diagrams show the differentiation trend in the Ahar Magmatic Com-

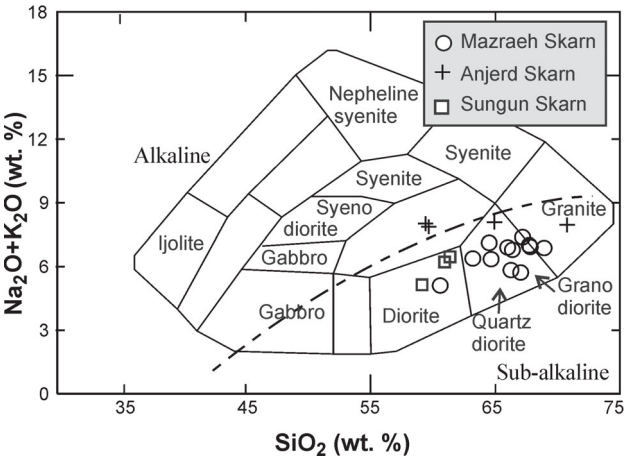

Fig. 8. Plot of Na_2O+K_2O vs. SiO_2 for igneous rocks of the Ahar region after Wilson (1989).

Table 5: Representative chemical analysis of major (wt. %) and trace elements (ppm) for igneous rocks of the Ahar region NW Iran.

Sample	A11	A17	A18	Z28a	Z28b	Z28e	MZ52	MZ54	MZ78	MZ77	MZ310	MZ81
SiO_2	63.23	60.63	66.27	67.73	66.02	67.05	67.20	68.92	67.81	64.54	64.69	66.39
Al_2O_3	15.02	15.56	13.77	14.73	15.91	15.16	14.70	14.91	14.95	15.90	15.00	15.78
TiO_2	0.30	1.03	1.25	0.74	0.87	0.62	0.49	0.38	0.58	0.69	0.87	0.67
FeO	3.19	3.07	3.00	2.85	3.31	3.01	2.00	2.06	3.00	2.36	2.39	3.42
Fe_2O_3	1.66	2.27	2.18	0.74	0.97	0.53	0.68	0.33	0.44	1.63	2.14	1.47
MgO	2.35	3.08	1.18	1.23	2.61	1.90	1.72	1.30	1.77	2.20	2.61	2.13
CaO	4.64	7.61	3.87	3.86	4.38	4.46	4.64	2.78	3.40	4.09	4.61	3.71
MnO	0.10	0.09	0.11	0.07	0.63	0.10	0.04	0.03	0.04	0.07	0.07	0.06
K_2O	2.89	0.68	2.98	2.75	2.85	1.80	2.89	2.91	2.90	2.83	2.99	2.98
Na_2O	3.47	4.41	2.83	4.23	4.03	3.90	4.46	3.95	4.00	4.26	3.34	3.79
P_2O_5	0.45	0.62	0.12	0.26	0.47	0.42	0.32	0.30	0.40	0.47	0.53	0.44
CO_2	1.47	0.72	1.49	0.18	0.44	0.02	0.13	0.46	0.38	1.55	0.16	0.13
H_2O+	0.90	0.28	0.56	0.72	0.00	0.71	0.57	0.49	0.50	0.10	0.77	0.78
H_2O-	0.49	0.80	0.15	0.22	0.03	0.16	0.09	0.04	0.03	0.05	0.03	0.21
Ag	8	13	0	12	13	11	2	0	10	15	15	10
Cr	0	63	21	93	68	55	126	59	75	101	83	80
Co	32	41	29	29	36	14	26	19	27	27	44	24
Ni	31	103	59	58	71	35	156	99	95	94	126	94
Cu	380	195	160	5171	116	152	446	86	161	143	190	201
Zn	87	120	103	81	85	51	65	60	67	105	70	86
La	64	92	100	47	71	66	61	62	73	57	99	66
Pb	55	114	74	82	54	82	52	58	58	72	44	58
Cd	10	1	7	5	4	10	11	4	2	4	5	8
Ba	893	337	476	266	720	675	446	563	576	602	859	828
Mo	48	46	33	43	45	42	33	35	35	38	16	40
W	139	140	108	133	139	137	106	128	111	118	121	116
LI	2	30	8	43	14	10	8	303	28	22	21	21
Ga	52	0	28	296	9	24	86	0	23	5	27	13
Rb	139	91	151	92	120	139	161	149	144	122	155	149
Sr	557	824	438	618	753	658	627	672	667	779	692	733
Zr	224	153	15	126	200	168	151	144	194	208	192	212
Nb	19	15	110	62	26	25	22	23	27	23	29	27
Th	15	7	43	19	23	29	29	33	43	18	28	22
Y	13	0	15	12	5	10	14	13	12	2	12	6
U	3	2	9	5	6	9	8	8	11	6	7	7

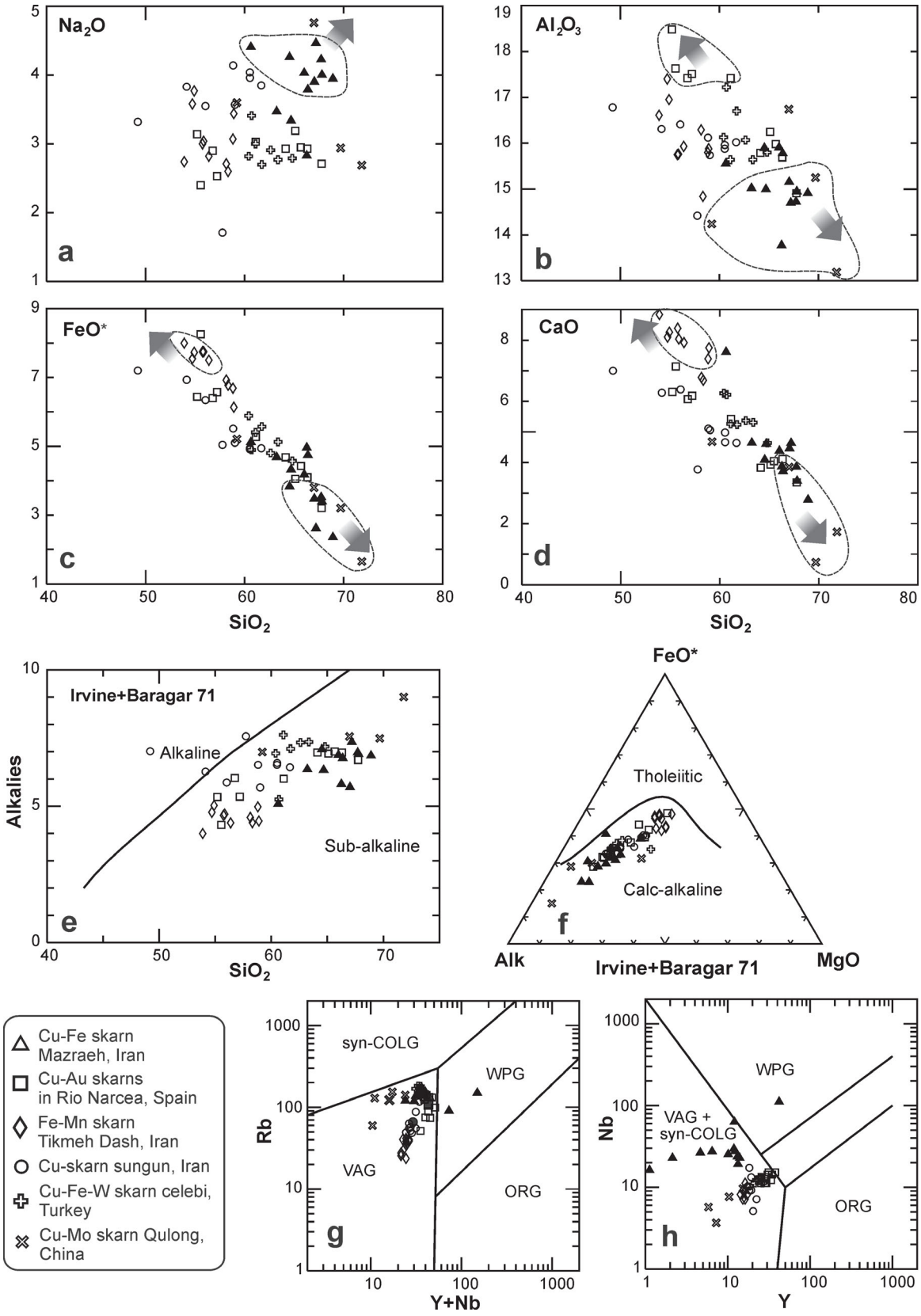

Fig. 9. a–d — Harker diagrams of SiO_2 vs. major oxides of Na_2O, Al_2O_3, FeO and CaO respectively; **e** — Variation diagram of SiO_2 vs. Alkalis; **f** — AFM diagram (after Irvine & Baragar 1991). In both e and f — the rocks are located in the calcalkaline and subalkaline fields; **g, h** — Variation diagrams of Y vs. Nb + Y and Y vs. Nb after Pearce (1996) to show geotectonic environment of the magmas. Most of data from the study area are located in the volcanic arc field.

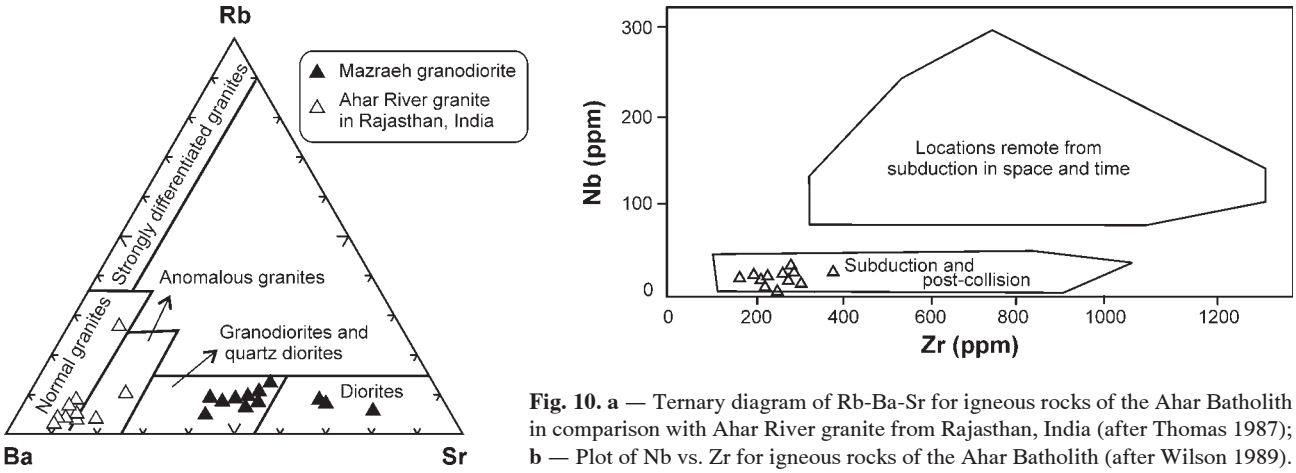

Fig. 10. a — Ternary diagram of Rb-Ba-Sr for igneous rocks of the Ahar Batholith in comparison with Ahar River granite from Rajasthan, India (after Thomas 1987); **b** — Plot of Nb vs. Zr for igneous rocks of the Ahar Batholith (after Wilson 1989).

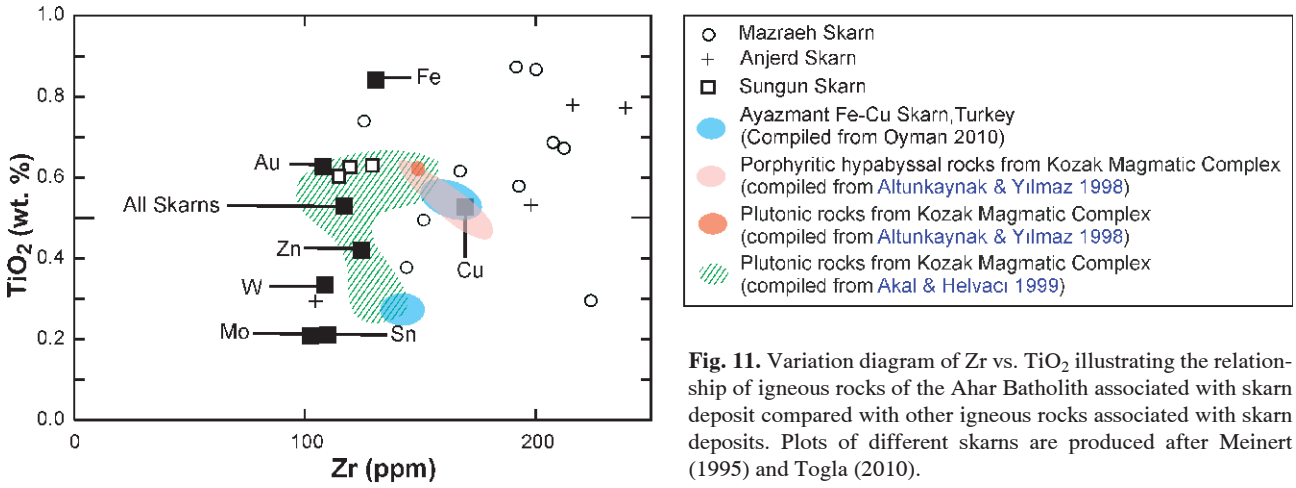

Fig. 11. Variation diagram of Zr vs. TiO_2 illustrating the relationship of igneous rocks of the Ahar Batholith associated with skarn deposit compared with other igneous rocks associated with skarn deposits. Plots of different skarns are produced after Meinert (1995) and Togla (2010).

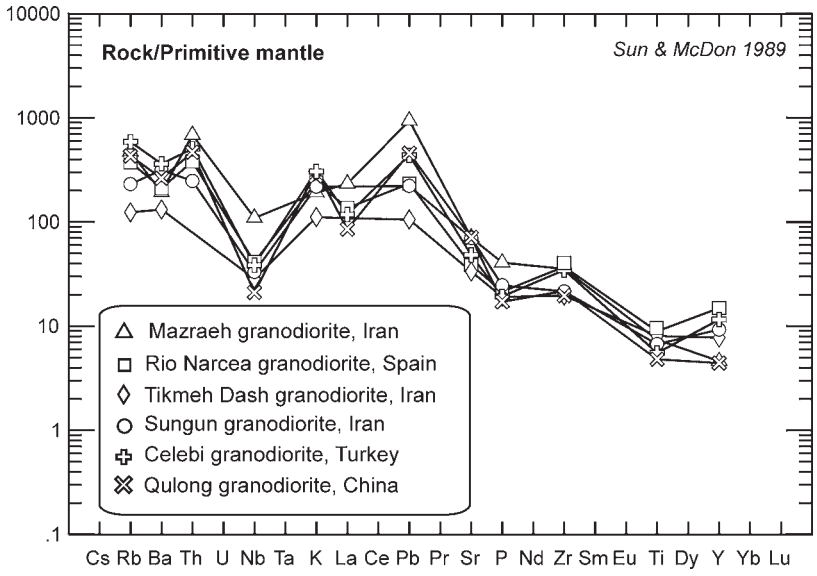

Fig. 12. Primitive mantle-normalized, incompatible trace-elements spider diagram for Mazraeh, Sungun and Tikmeh dash granodiorites (NW Iran), Rio Narcea Granodiorite (Spain), Celebi Granodiorite (Turkey) and Qulong Granodiorite (China). Normalizing data for all elements are from Sun & McDonough (1989). For data sources, see text.

plex in comparison with the Ahar river granite in Rajasthan, India (Fig. 10a). The Nb vs Zr diagram, only for the Mazraeh granodiorite, shows post collision and subduction-related characteristics (Fig. 10b). On the TiO_2 vs. Zr diagram, the plutonic rocks associated with Cu and Au skarns plot in the area between plutons associated with Cu and Au skarns, as proposed by Meinert (1995) and Oyman (2010) (Fig. 11). However the other porphyritic igneous rocks plot near the igneous rocks associated with Cu- and Fe skarns. Comparison of Ahar granodiorite with other granodiorites like the Qulong granodiorite of China (Xiao et al. 2012), the Rio Narcea belt in Spain (Martin-Izard et al. 2000), the Celebi pluton in Turkey (Kuşcu et al. 2002), and monzonite-granodiorite association of Khankandi pluton, Alborz Mountains, NW Iran (Aghazadeh et al. 2010) indicate that the Mazraeh granodiorites are enriched in elements like Th, Nb, La, P,

Table 6: Averages of major oxide concentrations for various groups of rocks in the Ahar region, NW Iran. Numbers correspond to the zones shown in Fig. 13.

Oxide	1. Igneous	2. Endoskarn	3. Internal ore	4. Exoskarn	5. Outer ore	6. Crystalline limestone
SiO_2	6.87	52.92	20.24	36.70	28.66	18.11
Al_2O_3	15.11	15.85	1.38	7.80	3.76	5.37
TiO_2	0.68	1.00	0.16	0.92	0.18	0.26
FeO	2.50	2.38	14.55	5.65	11.75	1.05
Fe_2O_3	1.30	4.72	50.64	15.52	42.30	1.38
MgO	2.01	2.09	1.52	4.29	1.74	1.33
CaO	4.34	11.29	1.52	23.60	1.50	43.52
MnO	0.15	0.30	4.91	0.56	1.26	0.12
K_2O	2.73	1.82	0.29	0.35	0.23	0.62
Na_2O	3.89	3.35	0.22	0.60	0.46	0.67
P_2O_5	0.39	0.50	3.50	0.71	2.05	0.18
L.O.I	0.59	1.29	1.54	1.02	0.25	27.10

Cu and Pb (Fig. 12). Copper in the Ahar batholith ranges from 86 ppm to 5171 ppm with average of 607 ppm (Tables 5 and 6). This indicates the original magma was rich in Cu.

Discussion

Evolution of the skarn deposits

Skarn deposit mineralogy is spatially zoned with respect to pluton contacts, host rock lithology, and (or) fluid pathways. The prograde stage is temporally and spatially divided into two sub-stages: (a) metamorphic–bimetasomatic (sub-stage I) and (b) prograde metasomatic (sub-stage II). Sub-stage I began immediately after the intrusion of the pluton into the enclosing impure carbonates. Sub-stage II commenced with segregation and evolution of a uid phase in the pluton and its invasion into fractures and micro-fractures of the marmorized and skarnoid-hornfelsic rocks developed during sub-stage I. From texture and mineralogy the retrograde metasomatic stage can be divided into two discrete sub-stages: (a) early (sub-stage III) and (b) late (sub-stage IV). During sub-stage III, the previously formed skarn zones were affected by intense multiple hydro-fracturing phases in the Cu-bearing stock. In addition to Fe, Si and Mg, substantial amounts of Cu, Pb, Zn, along with volatile components such as H_2S and CO_2 were added to the skarn system. Consequently considerable amounts of hydrous calc-silicates (epidote, tremolite-actinolite), sulphides (pyrite, chalcopyrite, galena, sphalerite, bornite), oxides (magnetite, hematite) and carbonates (calcite, ankerite) replaced the anhydrous calc-silicates. Sub-stage IV was concurrent with the incursion of relatively low temperature, more highly oxidizing uids into the skarn system, bringing about partial alteration of the early-formed calc-silicates and developing a series of very ne-grained aggregates of chlorite, clay, hematite and calcite.

In the Ahar region the processes that lead to the formation of skarn deposits include three stages as follows (Table 7):

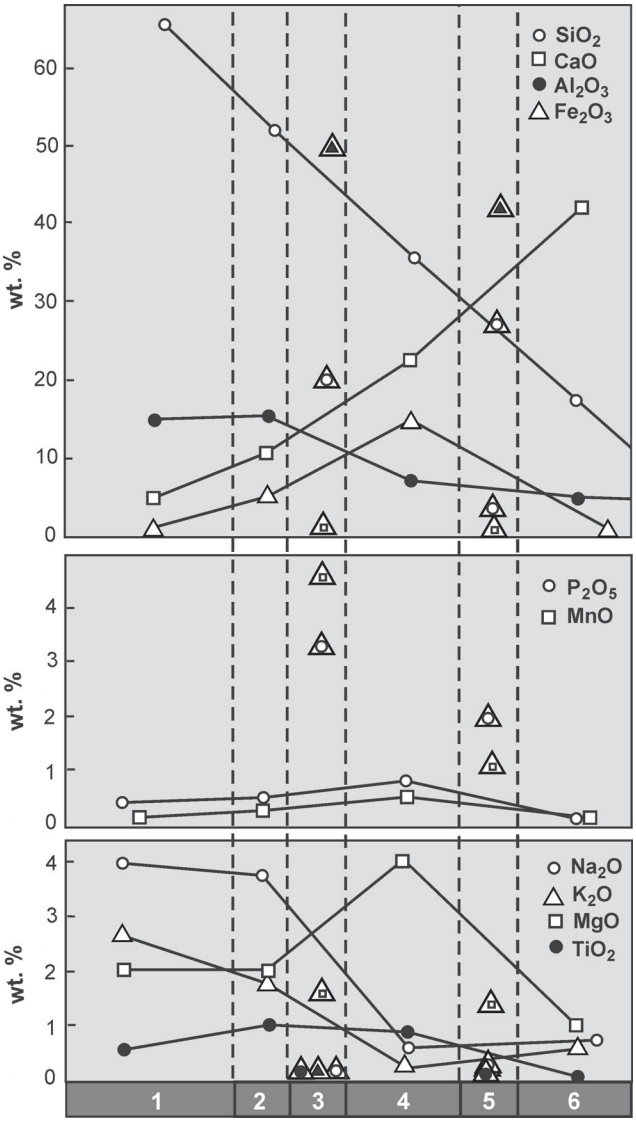

Fig. 13. Spatial variation diagram for average major oxide content in different rock types in skarns of the Ahar Batholith. **1** — Igneous rock, **2** — Endoskarn, **3** — Internal ore, **4** — Exoskarn, **5** — Outer ore, **6** — Crystalline limestone.

(1) Emplacement of plutonic magma which leads to the isochemical contact metamorphism;

(2) prograde metasomatic skarn formation as the pluton cools and an ore fluid develops, and;

(3) retrograde alteration of earlier formed mineral assemblages, leading to the formation of hydrosilicate minerals along with ore deposition. The third stage can also be divided into two sub-stages. In the other words, the total stages of skarn deposit and related hydrothermal activities can be considered in five stages. Calagari & Hosseinzadeh (2006a) believed that the skarnication process occurred in two stages: (1) prograde and (2) retrograde and each stage is temporally and spatially divided into sub-stages.

In the Ahar region, (1) the first stage commenced with the emplacement, consolidation and crystallization of the magma. As crystallization progressed the volume of hydrothermal

Table 7: Simplified paragenetic sequence of minerals present in the various rock types of the Ahar Region, NW Iran.

Minerals	Initial stage	Prograde stage	Prograde stage				Supergene
	Igneous and carbonate rocks	Stage 1	Stage 2	Stage 3	Stage 4	Stage 5	
Calcite							
Garnet							
Pyroxene							
Hornblende							
Plagioclase							
Wollastonite							
Epidote							
Actinolite							
Biotite							
Orthoclase							
Sphene							
Chlorite							
Rutile							
Magnetite							
Hematite							
Chalcopyrite							
Pyrite							
Galena							
Sphalerite							
Bornite							
Siderite							
Ankarite							
Malachite							
Azurite							
Siderite							
Quartz							
Muscovite							
Clay minerals							

fluid, generated and evolved, increased in the still-unconsolidated magma. The loss of CO_2 and H_2O during these processes caused a net volume loss and increased porosity (Rose & Burt 1979). Numerous fractures and veins were formed due to this invasion, this was the ground preparation for later events and the movement of mineralizing fluids.

(2) The second stage is the main stage of metasomatic (prograde metasomatic stage) marked by the growth of anhydrous minerals like garnet and pyroxene and the development of a volatile-rich phase (Candela & Piccoli 1995). Some workers like Burnham (1979), Cline & Bodnar (1991) and Hedenquist et al. (1998) have modelled the exsolution of a volatile phase from the magma and the partitioning of metals and chlorine between the melt and a volatile phase. During the prograde stage, the aqueous phase in the magma gradually became saturated and exsolved as a separate phase (based on Bowen series reaction), so that the unconsolidated proportion of magma actually increased due to involvement of hydrothermal fluid. The introduction of considerable amounts of Fe, Si and Mg from magma and Ca from crystalline carbonate rocks led to the development of substantial amounts of medium to coarse-grained anhydrous calc-silicates near the contact to produce the typical endoskarn and exoskarn toward the igneous and metamorphic sediments respectively. The anhydrous calcsilicate assemblages in the prograde stage of skarn formation can be correlated with the characteristic alteration in the mineralized part of the pluton that is in the contact zone (Meinert 1992; Kwak 1994). The fluid inclusion data from the igneous rocks indicate that the temperature of these magma-derived fluids (which is thought to have been involved in potassic alteration) was conceivably 520 °C to 580 °C (Calagari 2004; Mollai et al. 2009) and caused the prograde metasomatic alteration, particularly in proximity to the intrusive contact. Almost the same temperature, 600 °C, was reported for such a prograde stage from fluid inclusion studies in the calcic skarn hosting the El Valle-Boinas copper-gold deposit in Spain (Cepedal et al. 2000).

The minerals in the skarn zone belong to the system CaO–Al_2O_3–Fe_2O_3–SiO_2–H_2O and the system CaO–MgO–FeO–SiO_2–H_2O so that the final mineralogy is a combination of the two series of reaction in the endoskarn.

Plagioclase → Epidote → Garnet

Biotite → Amphibole → Clinopyroxene

(3) The third stage represents, therefore, the culmination of the prograde skarn formation and is followed by a drop in temperature and beginning of the retrograde stages of skarn formation. The crystallization of epidote, chlorite, tremolite–actinolite, and sphene characterize this initial retrograde stage. The chalcopyrite follows magnetite by replacing it and the earlier minerals such as garnet, calcite, and hematite. Processes such as hydrolysis, carbonation and sulphidation, due to relatively low temperature hydrothermal fluids, were responsible for the formation of these mineral assemblages. Epidote is the most common alteration mineral, locally ranging from 50 to 85 % in modal value. A local increase in fO_2 may have played an important role in the formation of epidote (Perkins et al. 1986; Berman 1988):

$$\underset{\text{garnet}}{Ca_3(Fe,Al)_2Si_3O_{12}} + {}^{5}/_{4}O_2 + HCO_3 \Rightarrow CaCO_3 + \underset{\text{epidote}}{Ca_2FeAl_2Si_3O_{12}} + {}^{1}/_{2}Fe_2O_3$$

Tremolite–actinolite in this sub-stage was probably formed by retrograde alteration of clinopyroxene (Zussman et al. 1992). Such alteration is well illustrated where the remnants of pyroxene and garnet are seen within the actinolite minerals (Mollai et al. 2009):

$$\underset{\text{clinopyroxene}}{Ca(Fe,Mg)_2Si_2O_6} + 2H_2O + 3CO_2 \Rightarrow \underset{\text{tremolite–actinolite}}{Ca_2(Fe,Mg)_5Si_8O_{22}(OH)_2} + CaCO_3 + 2SiO_2$$

Thus, at least two paragenetic stages of skarn formation and ore deposition have been recognized: stage 2, hedenbergitic pyroxene ± garnet ± scapolite (meionite) ± quartz ± magnetite, and stage 3 amphibole ± epidote ± chlorite ± quartz co ± calcite and pyrrhotite + chalcopyrite ± pyrite. The hydrous skarn assemblage (stage 3) replaced early-formed skarn assemblages. This alteration is similar to the other Cu-Fe and Fe-Cu skarn deposits in the world (Meinert 1992; Kwak 1994; Newberry 1998; Meinert et al. 2005; Yücel Öztürk et al. 2008).

(4) The magnetite-chalcopyrite metasomatism is followed by epigenetic hydrothermal veins containing chalcopyrite, bornite, covellite, cubanite, magnetite, quartz, calcite and chlorite. The veins filled a system of conjugate fractures transverse to the original bedding direction.

(5) The latest episode in the area is represented by the barren hydrothermal veins containing quartz, calcite and/or chlorite veinlets and alteration of the existing low temperature assemblage minerals to epidote, chlorite, and carbonates.

According to Einaudi et al. (1981), the distribution, mineralogy and metal ratios of skarns are quite variable, and may be correlated to the types of magma, depth of formation, oxidation state and distance from intrusion (Meinert 1995). The different oxygen fugacities within the magma and liberated ore solution are essential for the development of a metallogenic province. According to Einaudi et al. (1981), magnetite-rich skarn, equivalent to the Fe-Co skarn of Smirnov et al. (1976) and Smirnov & Beus (1983), with significant Cu, Co and Au content, was produced from more mafic igneous rock types of an oceanic island arc. A hypabyssal environment produces Fe, Cu, Mo, Pb and Zn skarn. Lithophile mineralized skarns like Sn, W, F, Li, Be, and B are confined to belts of highly siliceous alkalic granites, whereas litho-chalcophile mineralization (W, Ho, Cu, Zn, Pb, Au, Hg, Sb) is more typical of moderately siliceous magmas.

The arc-magmatic or subduction-related setting of these granodioritic rocks are indicated by their major and trace-element geochemistry (Figs. 8, 9, 10). Magnetite-bearing epidote-pyroxene, plagioclase, garnet endoskarn and garnet-epidote bearing exoskarn are characteristic of island-arc skarn (Einaudi et al. 1981). The andraditic garnet is the main skarn mineral and pyroxene belongs to the diopside-hedenbergite series. Magnetite is the dominant primary iron oxide mineral, occurring either between exoskarn and limestone or endoskarn and exoskarn. Chalcopyrite and pyrite are the important sulphide minerals, as in the Shinyama mine, Kamaishi district, Japan, which is an island-arc type of skarn deposit. The most characteristic retrograde minerals include epidote, actinolite, chlorite, calcite and quartz. Copper skarns reported from oceanic island arc settings associated with quartz monzonite to granodiorite plutons are characterized by high garnet to pyroxene ratios, relatively oxidized assemblages (andraditic garnet, diopside, pyroxene, magnetite and hematite) and moderate to high sulphide content (Meinert 1984). From the above discussion and comparison, it can be concluded that the island-arc setting is very well fitted to the skarn deposits in the Ahar region and the ore solution related to their magmatic origin.

Conclusions

The skarn deposits of the Ahar region can be classified petrologically into endoskarn, exoskarn and ore skarn. Each of these can be further subdivided on the basis of predominant mineral assemblage. The dominant skarn minerals are garnet, calcite, pyroxene, actinolite and epidote which are accompanied by quartz, feldspar, minor vesuvianite and hornblende. These early-formed calc-silicate minerals were later texturally replaced by oxides (magnetite, hematite), sulphides (chalcopyrite, pyrite, covellite, bornite, galena, sphalerite) and carbonates (calcite, ankerite and siderite). Field evidence, mineralogical and textural criteria and compositional data show five stages of skarn evolution. The first stage consists of plutonic emplacement and iso- chemical metamorphism, followed by the prograde metasomatic stage, marked by the growth of anhydrous minerals (pyroxene and garnet). The third stage of the skarn formation is marked by magnetite replacing anhydrous calc-silicate minerals. The fourth stage is marked by a drop in temperature and the beginning of the retrograde changes. Magnetite-chalcopyrite metasomatism is followed by epigenetic hydrothermal veins containing chalcopyrite, bornite, covellite, cubanite, magnetite, quartz, calcite and chlorite. The last stage is represented by barren hydrothermal quartz veins, veinlets of calcite and/or chlorite, and alteration of the existing low temperature assemblage minerals to epidote, chlorite and carbonates.

Spatial and temporal association of mineral deposits with island-arc setting related magmatic activity in the Ahar region of NW Iran allow us to define metallogenic epochs and

petrographical to geochemical provinces that could be used in mineral exploration. Temporal association of Cu-Mo, Cu and Cu-Fe skarn deposits with post-collisional granitoids suggest a metallogenic epoch during the Oligo-Miocene in northwest and central Iran (Sarcheshmeh copper porphyry in Kerman). In this epoch, formation of Cu and Cu-Fe skarn deposits took place in the province of granodioritic intrusions, and Cu-Mo deposits were formed in the province of monzonitic to monzodioritic intrusions. The most significant feature assigned to the island arc setting and post- collision granitoids in the Ahar region is that they are products of homogeneous to heterogeneous mixing melt formed in a single tectonic setting. From the above discussion and comparison, it can be concluded that the calc-alkaline, volcanic arc geochemistry of the host granodiorite and the mineralogical assemblages in the skarns suggest that the skarn deposits of the Ahar region formed in an island-arc subduction setting.

Acknowledgments: We gratefully acknowledge the financial support for this research made available by the Vice Presidency of Research and Technology, Mashhad Branch, Islamic Azad University Mashhad, Iran. I would like to offer special thanks to my friend, Dr. A. Fazelli, in GSI, Dr K. Rostamy in Germany and Eng. R. Sharifian for their very helpful suggestions and constructive criticisms.

References

Aghanabati A. 1993: Geological survey of Iran Geological quadrangle map of Iran No. J11 (Bam sheet), scale, 1:250,000.

Aghazadeh M., Castro A., Omran N.R., Emami M.H., Moinvaziri H. & Badrzadeh Z. 2010: The gabbro (shoshonitic)–monzonite–granodiorite association of Khankandi pluton, Alborz Mountains, NW Iran. *J. Asian Earth Sci*. 38, 5, 199–219.

Atkinson W. & Einaudi M. 1978: Skarn formation and mineralization in the contact aureole at Carr Fork, Bingham, Utah. *Econ. Geol*. 73, 7, 1326–1365.

Azizi H. & Moinevaziri H. 2009: Review of the tectonic setting of Cretaceous to Quaternary volcanism in northwestern Iran. *J. Geodynamics* 47, 4, 167–179.

Bazin D. & Hübner H. 1969: Copper deposits in Iran. *Geol. Surv.* Iran, Teheran, 1–226.

Berman R. 1988: Internally-consistent thermodynamic data for minerals in the system Na_2O-K_2O-CaO-MgO-FeO-Fe_2O_3-Al_2O_3-SiO_2-TiO_2-H_2O-CO_2. *J. Petrology* 29, 2, 445–522.

Boztuğ D., Kuşçu İ., Erçin A., Avcı N. & Şahin S. 2003: Mineral deposits associated with the pre-, syn-and post-collisional granitoids of the Neo-Tethyan convergence system between the Eurasian and Anatolian plates in NE and Central Turkey. Mineral exploration and sustainable development. *Millpress*, Rotterdam, 1141–1144.

Burnham C.W. 1979: Magmas and hydrothermal fluids. *Geochem. Hydrothermal Ore Deposits* 2, 71–136.

Calagari A.A. 2004: Fluid inclusion studies in quartz veinlets in the porphyry copper deposit at Sungun, East-Azarbaidjan, Iran. *J. Asian Earth Sci.* 23, 2, 179–189.

Calagari A.A. & Hosseinzadeh G. 2006a: The mineralogy of copper-bearing skarn to the east of the Sungun-Chay river, East-Azarbaidjan, Iran. *J. Asian Earth Sci.* 28, 4–6, 423–438.

Calagari A.A. & Hosseinzadeh G. 2006b: The mineralogy of copper-bearing skarn to the east of the Sungun-Chay river, East-Azarbaidjan, Iran. *J. Asian Earth Sci*. 28, 4, 423–438.

Candela P. & Piccoli P. 1995: Model ore-metal partitioning from melts into vapor and vapor/brine mixtures. *Magmas, Fluids, and Ore Deposits* 23, 101–127.

Cepedal A., Martín-Izard A., Reguilón R., Rodrıguez-Pevida L., Spiering E. & González-Nistal S. 2000: Origin and evolution of the calcic and magnesian skarns hosting the El Valle-Boinás copper–gold deposit, Asturias (Spain). *J. Geochem. Explor*. 71, 2, 119–151.

Chen Y.-J., Chen H.-Y., Zaw K., Pirajno F. & Zhang Z.-J. 2007: Geodynamic settings and tectonic model of skarn gold deposits in China: an overview. *Ore Geol. Rev*. 31, 1, 139–169.

Cline J.S. & Bodnar R.J. 1991: Can economic porphyry copper mineralization be generated by a typical calc-alkaline melt? *J. Geophys. Res*. 96, B5, 8113–8126.

Dilek Y., Imamverdiyev N. & Altunkaynak Ş. 2010: Geochemistry and tectonics of Cenozoic volcanism in the Lesser Caucasus (Azerbaijan) and the peri-Arabian region: collision-induced mantle dynamics and its magmatic fingerprint. *Int. Geol. Rev*. 52, 4–6, 536–578.

Einaudi M.T. & Burt D.M. 1982: Introduction; terminology, classification, and composition of skarn deposits. *Econ. Geol.* 77, 4, 745–754.

Einaudi M., Meinert L. & Newberry R. 1981: Skarn deposits. *Econ. Geol*., 75th Anniv., Vol. 317–391.

Etminan H. 1978: Discovery of copper and Molybdenum porphyry near Sungun village NW Iran. *Report Geol. Surv*., Iran, 1–1356.

Groves D.I., Goldfarb R.J., Gebre-Mariam M., Hagemann S. & Robert F. 1998: Orogenic gold deposits: a proposed classification in the context of their crustal distribution and relationship to other gold deposit types. *Ore Geol. Rev*. 13, 1, 7–27.

Hedenquist J.W., Arribas A. & Reynolds T.J. 1998: Evolution of an intrusion-centered hydrothermal system; Far Southeast-Lepanto porphyry and epithermal Cu-Au deposits, Philippines. *Econ. Geol*. 93, 4, 373–404.

Hezarkhani A., Williams-Jones A. & Gammons C. 1999: Factors controlling copper solubility and chalcopyrite deposition in the Sungun porphyry copper deposit, Iran. *Mineralium Depos*. 34, 8, 770–783.

Hezarkhani A. & Williams-Jones A.E. 1998: Controls of alteration and mineralization in the Sungun porphyry copper deposit, Iran; evidence from fluid inclusions and stable isotopes. *Econ. Geol*. 93, 5, 651–670.

Hollister L.S. & Crawford M.L. (Eds.) 1981: Fluid inclusions: Applications to petrology. *Miner. Assoc*. Canada, Ontario, Short Course Handbook, 6, 1–304.

Jamali H., Dilek Y., Daliran F., Yaghubpur A. & Mehrabi B. 2010: Metallogeny and tectonic evolution of the Cenozoic Ahar–Arasbaran volcanic belt, northern Iran. *Int. Geol. Rev*. 52, 4–6, 608–630.

Karimzadeh Somarin A. 2004: Garnet composition as an indicator of Cu mineralization: evidence from skarn deposits of NW Iran. *J. Geochem. Explor*. 81, 1, 47–57.

Kuşcu I., Gençalioğlu Kuşcu G., Meinert L.D. & Floyd P.A. 2002: Tectonic setting and petrogenesis of the Çelebi granitoid, (Kırıkkale-Turkey) and comparison with world skarn granitoids. *J. Geochem. Explor*. 76, 3, 175–194.

Kwak T.A.P. 1994: Hydrothermal alteration in carbonate-replacement deposits; ore skarns and distal equivalents. Alteration and alteration processes associated with ore-forming systems: *Geol. Assoc. Canada Short Course Notes* 11, 381–402.

Kwak T.A.P. & Kwak T. 1987: W-Sn skarn deposits and related metamorphic skarns and granitoids. *Elsevier*, Amsterdam, 1–439.

Lescuyer J.I. & Riou R. 1976: Géologie de la région de Mianeh (Azarbaijan). Contribution de la volcanisme tertiare de l' Iran. *Thèse 3 cycle*, Grenoble, 1–234.

Martin-Izard A., Fuertes-Fuente M., Cepedal A., Moreiras D., Nieto

J.G., Maldonado C. & Pevida L.R. 2000: The Rio Narcea gold belt intrusions: geology, petrology, geochemistry and timing. *J. Geochem. Explor*. 71, 2, 103–117.

Mehrpartou M. 1993: Contributions to the geology, geochemistry, Ore genesis and fluid inclusion investigations on Sungun Cu-Mo porphyry deposit, northwest of Iran. *Ph.D. Dissertation, University of Hamburg*, Germany, 1–245.

Mehrpartou M. & Torkian M. 1994: Investigation on Fluid inclusion in Copper Molybdenum Porphyritic Complex of Sungun,West of Ahar, East Azerbaijan. *J. Geosci. Sci. Quart*. 3, 3–27.

Meinert L.D. 1984: Mineralogy and petrology of iron skarns in western British Columbia, Canada. *Econ. Geol*. 79, 5, 869–882.

Meinert L.D. 1992: Skarns and skarn deposit. *J. Geol. Assoc*. Canada, *Geosci.* Canada 19, 4, 145–162.

Meinert L.D. 1995: Compositional variation of igneous rocks associated with skarn deposits — Chemical evidence for a genetic connection between petrogenesis and mineralization. In: Thompson J.F.H. (Ed.): Magmas, fluids, and ore deposits. Miner. *Assoc. Canad. Short Course Ser*. 23, 401–418.

Meinert L., Dipple G. & Nicolescu S. 2005: World skarn deposits. *Econ. Geol*. 100, 299–336.

Mollai H. 1993: Petrochemistry and genesis of the granodiorite and associated iron-copper skarn deposit of Mazraeh, Ahar, East Azarbaijan, Iran. *Unpubl. PhD Thesis, University of Roorkee*, Roorkee, 1–265.

Mollaei H., Yaghubpur A. & Attar R.S. 2009: Geology and geochemistry of skarn deposits in the northern part of Ahar batholith, East Azarbaijan, NW Iran. *Iranian J. Earth Sci*. 1, 1, 15–34.

Mollai H., Sharma R. & Pe-Piper G. 2009: Copper mineralization around the Ahar batholith, north of Ahar (NW Iran): Evidence for fluid evolution and the origin of the skarn ore deposit. *Ore Geol. Rev*. 35, 3–4, 401–414.

Newberry R.J. 1998: W-and Sn-skarn deposits: a 1998 status report. *Mineral. Assoc. Canada, Short Course Ser.* 26, 289–335.

Oyman T. 2010: Geochemistry, mineralogy and genesis of the Ayazmant Fe–Cu skarn deposit in Ayvalik, (Balikesir), Turkey. *Ore Geol. Rev*. 37, 3, 175–201.

Perkins E., Brown T. & Berman R. 1986: PT-SYSTEM, TX-SYSTEM, PX-SYSTEM: three programs which calculate pressure-temperature-composition phase diagrams. *Computers & Geosciences* 12, 6, 749–755.

Rolland Y., Billo S., Corsini M., Sosson M. & Galoyan G. 2009: Blueschists of the Amassia-Stepanavan Suture Zone (Armenia): linking Tethys subduction history from E-Turkey to W-Iran. *Int. J. Earth Sci*. 98, 3, 533–550.

Rose A. & Burt D. 1979: Hydrothermal alteration. In: Barnes H.L. (Ed.): Geochemistry of hydrothermal ore deposits. *2nd edit. John Wiley* 8, 173–235.

Schwartz G.M. 1950: Problems in the relation of ore deposits to hydrothermal alteration. *Quart. J. Colo. School of Mines* 4, 197–208.

Smirnov V.I. & Beus A.A. 1983: Studies of mineral deposits. *MIR Publ.*, Moscow, 1–288.

Smirnov V.I., Creighton H.C. & Dunham K. 1976: Geology of mineral deposits. *MIR Publ.*, Moscow, 1–520.

Superceanu C. 1971: The eastern Mediterranian-Iranian alpine copper-molybdenum belt. *Soc. Mining Geol. Japan, Spec*. 3, 393–398.

Tarkhani M., Vossogi Abdeini M. & Baharvand N. 2010: An introduction to Calc-alkaline lamprophyres (Spessartites) at Saghez Area. *J. Sci. Islamic Azad Univ*. 20, 77, 237–251.

Xiao B., Qin K., Li G., Li J., Xia D., Chen L. & Zhao J. 2012: Highly oxidized magma and fluid evolution of Miocene Qulong Giant Porphyry CuMo Deposit, Southern Tibet, China. *Res. Geol*. 62, 1, 4–18.

Yücel Öztürk Y., Helvacı C. & Satır M. 2008: The influence of meteoric water on skarn formation and late-stage hydrothermal alteration at the Evciler skarn occurrences, Kazdağ, NW Turkey. *Ore Geol. Rev*. 34, 3, 271–284.

Zussman J., Howie R. & Deer W. 1992: An introduction to the rock forming minerals. *Longman*, Harlow, (2nd edition), 1–712.